Atmósfera (1990), **3**, pp. 73-109

On the structure of transient atmospheric waves. Part III

A. WIIN-NIELSEN

Geophysical Institute, University of Copenhagen, Denmark

H. MARSHALL

Dept. of Atmospheric, Oceanic and Space Sciences, University of Michigan, Ann Arbor, Michigan, E. U.

(Manuscript received September 20, 1989; accepted in final form November 6, 1989)

RESUMEN

En el tercer y último artículo de la serie sobre la estructura relativa de las ondas atmosféricas transitorias consideramos un modelo de atmósfera con una continua especificación del viento zonal y de la estabilidad estática en el estado básico. Las variaciones verticales de los parámetros en el estado básico (excepto la estabilidad) y en las perturbaciones estarán representados como desarrollos en serie de funciones apropiadas a la variación vertical del parámetro de estabilidad estática.

Para la estabilidad consideraremos dos casos. El primero es una estabilidad estática constante en todo el modelo, y el segundo es un caso en el que la estabilidad varía inversamente proporcional al cuadrado de la presión. En el primer caso podemos usar funciones trigonométricas para describir las variaciones verticales. En el segundo caso derivamos las funciones de estructura apropiada, pero resulta que para satisfacer la condición en la frontera superior es necesario suponer que en dicha frontera la atmósfera tiene una presión mayor que cero.

La estructura relativa se obtiene en cada caso como una solución de las ecuaciones estacionarias para la amplitud relativa y el ángulo de fase relativo. Tales soluciones se obtienen directamente en casos simples, pero en casos más complicados mediante integraciones numéricas llevadas a cabo hasta que se llega a un estado estacionario.

ABSTRACT

In the third and final paper in the series on the relative structure of transient atmospheric waves we consider a model atmosphere with a continuous specification of the zonal wind and the static stability in the basic state. The vertical variations of the parameters in the basic state (except the stability) and in the perturbations will be represented as series expansions in functions appropriate to the vertical variation of the static stability parameter.

For the stability we shall consider two cases. The first is a constant static stability in the whole model, and the second is a case where the stability varies as inversely proportional to the square of the pressure. In the first case we may use trigonometric functions to describe the vertical variation. In the second case we derive the appropriate structure functions in the paper, but it turns out that to satisfy the upper boundary condition it is necessary to assume that the top of the atmosphere is located at a pressure larger than zero.

The relative structure is in each case obtained as a solution to the stationary equations for the relative amplitude and the relative phase angle. Such solutions are in simple cases obtained directly, but in more complicated cases by numerical integrations carried out to a point where an asymptotic steady state is obtained.

1. Introduction

In the first two papers, called I and II, we have considered the relative structure of transient atmospheric waves for the two -and three- level baroclinic models. The purpose of this paper is to generalize these studies to the purely baroclinic case with continuous vertical stratification. Such a study requires a specification of the vertical variation of the various parameters. The essential parameter in this connection is the static stability because it enters the equation determining the

vertical structure functions in quasi-geostrophic theory (Wiin-Nielsen, 1971). The first problem is therefore to adopt a specification of the variation of the static stability parameter with pressure. For a given specification we are required to seek a set of orthogonal functions which are solutions to the vertical structure equation. The general procedure thereafter is to develop the parameters in series of the orthogonal functions, to insert these series in the relevant equations, and to derive the equations for the time-dependent coefficients in the series of orthogonal functions. From these equations we can then proceed in a way analogous to the technique developed in I and II.

The main goal is to obtain the relative structure for the transient baroclinic waves. The advantage of the proposed procedure is that it will permit an arbitrary variation of the zonal wind in the basic current. The study will thus supplement other studies of the quasi-geostrophic, baroclinic stability problem, normally formulated as an eigenvalue problem which under these more general conditions will lead to extensive numerical calculations. The proposed methodology is not inexpensive in computations because the required relative structure should be obtained as a steady state of the equations for the relative amplitudes and phases of all the components. For a general situation with many components it is very difficult, if not impossible, to determine these steady states directly even by numerical methods due to the non-linearity in the governing equations. As a replacement it is proposed to integrate the equations in time to investigate whether or not an asymptotic steady state can be obtained. There is no guarantee that this will be the case for all parameter sets such as all wind-profiles and all wavelengths because the asymptotic solution may be oscillatory. However, if an asymptotic steady state is obtained we may be assured that it is stable, and the corresponding relative structure will consequently be observed.

In section 2 we start by considering a particularly simple case where the static stability parameter is constant. In that case the orthogonal functions are trigonometric, and this fact makes the evaluation of the interaction integrals completely straight forward. Section 3 will contain a general discussion of the structure equation and the possibilities to obtain orthogonal solutions. Section 4 will be the case where the static stability parameter varies as inversely proportional to the square of pressure, and Section 5 will treat a comparison between the continuous case and truncated case. Section 6 will be the concluding remarks.

2. The baroclinic case with constant static stability

I and II contain the most simple purely baroclinic cases, i.e., the two and three level, quasi-nondivergent models. In this section we shall reconsider the purely baroclinic case with a higher vertical resolution. It is known from baroclinic stability theory that the mathematical treatment becomes rather cumbersome if we include the vertical variation of the static stability $\sigma = -\alpha(\partial ln\theta/\partial p)$. From data studies conducted by Gates (1961) it is known how large this variation is. Jacobs and Wiin-Nielsen (1966) have used a basic state of the atmosphere characterized by a constant lapse rate. In this case one finds that $\sigma = \sigma(p_*)$, $p_* = p/p_0$ varies as $\sigma = \sigma_1 \; p_*^{-\lambda}$ where λ is a positive number which is less than 2 for realistic values of the lapse rate. The vertical variation of σ will have an influence on the vertical structure of the transient waves, but it is to be expected that the main feature of the structure may be obtained if one assumes that σ is constant with respect to pressure. In this case, as will be seen from this section, one may obtain results using elementary functions.

The quasi-nondivergent equations are:

$$\frac{\partial \varsigma}{\partial t}+\vec{V}\cdot\nabla(\varsigma+f)=\frac{f_o}{p_o}\frac{\partial \omega}{\partial p_*};\ p_*=\frac{p}{p_o};\ p_o=100kPa$$

$$\frac{\partial}{\partial t}[\frac{\partial \psi}{\partial p_*}]+\vec{V}\cdot\nabla[\frac{\partial \psi}{\partial p_*}]+\frac{\sigma p_o}{f_o}\omega=0 \tag{2.1}$$

with the boundary conditions that

$$\omega=0 \text{ at } p_*=0,\ p_*=1 \tag{2.2}$$

We shall also in this case need a reference state, and we select the vertical mean flow, also called the barotropic mode. For this purpose we introduce the definition:

$$(\ )_M=\int_o^1(\ )dp_*$$

$$(\ )_T=(\ )-(\ )_M \tag{2.3}$$

where the thermal flow, also called the vertical shear flow or the baroclinic component, is defined as the deviation of the total flow from the barotropic component. The definitions have been used extensively in the study of atmospheric energetics (Wiin-Nielsen, 1962).

(2.3) is applied to the first equation in (2.1) and using the boundary conditions (2.2) we find

$$\frac{\partial \varsigma_M}{\partial t}+\vec{V}_M\cdot\nabla\varsigma_M+(V_T\cdot\nabla\varsigma_T)_M+\beta V_M=0 \tag{2.4}$$

The vorticity equation for the baroclinic component is obtained by substracting (2.4) from the first equation in (2.1) with the result that

$$\frac{\partial \varsigma_T}{\partial t}+\vec{V}_M\cdot\nabla\varsigma_T+\vec{V}_T\cdot\nabla\varsigma_M+\vec{V}_T\cdot\nabla\varsigma_T-(\vec{V}_T\cdot\nabla\varsigma_T)_M+\beta V_T=\frac{f_o}{p_o}\frac{\partial \omega}{\partial p_*} \tag{2.5}$$

The vertical velocity in (2.5) may be eliminated in the usual way using the second equation in (2.1) and employing the assumption that $\sigma=\overline{\sigma}=$ const. We note that the stream function ψ appearing in the thermodynamic equation may be replaced by ψ_T since ψ_M by definition is independent of pressure. Introducing the potential vorticity

$$\xi_T=\varsigma_T+q^2\frac{\partial^2\psi_T}{\partial p_*^2};\ q^2=\frac{f_o^2}{\sigma p_o^2} \tag{2.6}$$

we obtain

$$\frac{\partial \xi_T}{\partial t}+\vec{V}_M\cdot\nabla\xi_T+\vec{V}_T\cdot\nabla\varsigma_M+\vec{V}_T\cdot\nabla\xi_T-(\vec{V}_T\cdot\nabla\varsigma_T)_M+\beta V_T=0 \tag{2.7}$$

In agreement with the treatment in the preceeding papers we specify the stream functions in the form

$$\psi_M(\mathrm{x},\ \mathrm{y},\ \mathrm{t}) = -U_M y + A_M(t)\ \cos\ kx + B_M(t)\ \sin\ kx$$

$$\psi_T(\mathrm{x},\ \mathrm{y},\ \mathrm{p}_*,\ \mathrm{t}) = -U_T(p_*)y + A_T(p_*,\ t)\ \cos\ kx + B_T(p_*,\ t)\ \sin\ kx \tag{2.8}$$

The next question of concern is how we shall specify the pressure dependence in U_T, A_T and B_T. Going back to (2.6) it is obvious that we can use a trigometric function. From the second equation in (2.1) we note that at the boundaries ($p_* = 0,\ p_* = 1$) we get

$$\frac{\partial}{\partial t}[\frac{\partial \psi_T}{\partial p_*}] + u\frac{\partial}{\partial x}[\frac{\partial \psi_T}{\partial p_*}] - \frac{\partial u_T}{\partial p_*}\frac{\partial \psi}{\partial x} = 0,\ p_* = 0,\ p_* = 1 \tag{2.9}$$

It is thus seen that (2.9) will be satisfied if we select a cos-dependence for U_T, A_T and B_T or, specifically:

$$U_T(p_*) = \sum_{q=1}^{\infty} U_T(q)\ \cos\ (q\pi p_*)$$

$$A_T(p_*,\ t) = \sum_{s=1}^{\infty} A_T(\mathrm{s},\ \mathrm{t})\ \cos\ (s\pi p_*)$$

$$B_T(p_*,\ t) = \sum_{s=1}^{\infty} B_T(\mathrm{s},\ \mathrm{t})\ \cos\ (s\pi p_*) \tag{2.10}$$

We note that the functions cos $(q\pi p_*)$ are orthogonal over the interval 0 to 1 because

$$\int_o^1 \cos(q\pi p_*)\ \cos\ (s\pi p_*)dp_* = \begin{cases} o & q \neq s \\ 1/2 & q = s \end{cases} \tag{2.11}$$

As a result of (2.11) it is for example seen that

$$(U_T A_T)_M = \frac{1}{2}\sum_{n=1}^{\infty} U_T(n)A_T(n) \tag{2.12}$$

and the corresponding relation for B_T.

After the specifications we proceed by substituting (2.8) in the equations (2.4) and (2.7). Following the same procedures as used in the previous papers and representing the amplitudes in the form

$$A_M = R_M \cos \theta_M, \quad B_M = R_M \sin \theta_M$$

$$A_T(n) = R_T(n) \cos \theta_T(n), \quad B_T(n) = R_T(n) \sin \theta_T(n) \tag{2.13}$$

and finally

$$r(n) = \frac{R_T(n)}{R_n}, \quad \delta(n) = \theta_M - \theta_T(n) \tag{2.14}$$

we may derive equations for $dr(n)/dt$ and $d\delta(n)/dt$. The procedure outlined above is cumbersome, but elementary from an algebraic point of view. The details will not be reproduced here. It will suffice to give the final result. The following notations will be used:

$$\Lambda = \pi^2 \frac{q^2}{k^2}$$

$$\gamma_1(n) = \frac{n^2\Lambda}{1+n^2\Lambda}$$

$$\gamma_2(n) = \frac{1-n^2\Lambda}{1+n^2\Lambda}$$

$$\gamma_3(n,\ s) = \frac{1-n(2s-n)\Lambda}{1+n^2\Lambda}$$

$$\gamma_4(n,\ s) = \frac{1+n(2s+n)\Lambda}{1+n^2\Lambda} \tag{2.15}$$

The equations are then:

$$\frac{dr(n)}{dt} = -k\gamma_2(n)U_T(n) \sin \delta(n) - \frac{1}{2}k \sum_{s=1}^{N} U_T(s)r(n)r(s) \sin \delta(s)$$

$$+\frac{1}{2}k\Bigg\{\sum_{s=1}^{n-1} \gamma_3(n,\ s)U_T(s)r(n-s) \sin\ [\delta(n-s) - \delta(n)]$$

$$+ \sum_{s=n+1}^{N} \gamma_3(n,\ s)U_T(s)r(s-n) \sin[\delta(s-n) - \delta(n)]$$

$$+ \sum_{s=1}^{N-1} \gamma_4(n,\ s)U_T(s)r(s+n) \sin\ [\delta(s+n) - \delta(n)]\Bigg\} \tag{2.16}$$

$$\frac{d\delta(n)}{dt} = -k\gamma_1(n)C_R - k\gamma_2(n)\frac{U_T(n)}{r(n)}\cos\,\delta(n) + \frac{1}{2}k\sum_{s=1}^{N} U_T(s)r(s)\cos\,\delta(s)$$

$$-\frac{1}{2}k\Bigg\{\sum_{s=1}^{n-1}\gamma_3(n,\ s)U_T(s)\frac{r(n-s)}{r(n)}\cos\,[\delta(n-s)-\delta(n)]$$

$$+\sum_{s=n+1}^{N}\gamma_3(n,\ s)U_T(s)\frac{r(s-n)}{r(n)}\cos[\delta(s-n)-\delta(n)]$$

$$+\sum_{s=1}^{N-n}\gamma_4(n,\ s)U_T(s)\frac{r(n+s)}{r(n)}\cos\,[\delta(s+n)-\delta(n)]\Bigg\} \tag{2.17}$$

The various terms in these equations may be categorized as follows:

1. The first term in (2.16) and the first two terms in (2.17) give the contribution from component n on its own changes.
2. The second term in (2.16) and the third in (2.17) measure the interaction between the barotropic and baroclinic component.
3. The three sums in each of the two equations measure the interaction between component n and the other components which can interact, i.e., those components having an index which give sums or differences of n as for example $s + (n - s) = n$.

It is obvious that the system (2.16) and (2.17) is so complicated that it would be out of the question to calculate all steady states in the general case. On the other hand, in the most simple case where we include one vertical component only we find no contribution at all from terms of category 3 and only one term from category 2. This case is analogous to the one considered in, the two level case. If we therefore want to use the system (2.16) and (2.17) we should either integrate it numerically to a stable steady state or design a case in which one may obtain steady states directly.

The latter possibility is used in the following example. For $U = U(p_*)$ we select a linear profile:

$$U(p_*) = U_1 + U_s(1 - p_*);\ U_1 = U(1) \tag{2.18}$$

Calculating the Fourier coefficients from the first expression in (2.10) we obtain

$$U_T(n) = \begin{cases} 0 & n \quad \text{even} \\ \frac{4U_s}{n^2\pi^2} & n \quad \text{odd} \end{cases}$$

If we further restrict the representation of the waves to odd components (i.e. $r(n) = \delta(n) = 0,\ n$ even) which are asymmetric around $p_* = \frac{1}{2}$, we observe that all terms in category 3 vanish because $s - n,\ n - s,\ n + s$ all are even, when n and s are odd. Consequently, we have contributions only from terms of categories 1 and 2. Restricting the number of vertical components to two we find the following equations:

$$\frac{dr(1)}{dt} = -k\gamma_2(1)U_T(1)\ \sin\ \delta(1) - \frac{1}{2}kU_T(1)r(1)^2\ \sin\ \delta(1) - \frac{1}{2}kU_T(3)r(1)r(3)\ \sin\ \delta(3)$$

$$\frac{dr(3)}{dt} = -k\gamma_2(3)U_T(3)\ \sin\ \delta(3) - \frac{1}{2}kU_T(1)r(1)r(3)\ \sin\ \delta(1) - \frac{1}{2}kU_T(3)r(3)^2\ \sin\ \delta(3)$$

$$\frac{d\delta(1)}{dt} = -k\gamma_1(1)C_R - k\gamma_2(1)\frac{U(1)}{r(1)}\ \cos\ \delta(1) + \frac{1}{2}kU_T(1)r(1)\ \cos\ \delta(1) + \frac{1}{2}kU_T(3)r(3)\ \cos\ \delta(3)$$

$$\frac{d\delta(3)}{dt} = -k\gamma_1(3)C_R - K\gamma_2(3)\frac{U_r(3)}{r(3)}\ \cos\ \delta(3) + \frac{1}{2}kU_T(1)r(1)\ \cos\ \delta(1)$$

$$+\frac{1}{2}kU_T(3)r(3)\ \cos\ \delta(3) \tag{2.20}$$

The system (2.20) corresponds to a model with three levels. In this case it is possible to solve the steady state problem by setting all four time-derivatives to zero. The solution requires a process of elimination, which is quite elementary. The results are:

$$r(3)^2 = 2\left[\frac{\Lambda-1}{\Lambda+1} - r(1)^2\right]\cdot\frac{(9\Lambda-1)(\Lambda+1)}{(9\Lambda+1)(\Lambda-1)}$$

$$\cos\ \delta(1) = \frac{2\Lambda\cdot C_R\cdot r(1)\left[1-\frac{4}{9\Lambda-1}r(3)^2\right]}{U_T(1)\left[(\Lambda+1)r(1)^2 + 2(\Lambda-1) + \frac{(\Lambda-1)(9\Lambda+1)}{(9\Lambda-1)}r(3)^2\right]} \tag{2.21}$$

$$\sin\ \delta(3) = 9\cdot\frac{(\Lambda-1)(9\Lambda+1)}{(\Lambda+1)(9\Lambda-1)}\frac{r(3)}{r(1)}\ \sin\ \delta(1)$$

$$a_6 r(1)^6 + a_4 r(1)^4 + a_2 r(1)^2 - a_o = 0$$

where

$$a_6 = \frac{32\Lambda^2}{(\Lambda-1)(81\Lambda^2-1)}$$

$$a_4 = \frac{8\Lambda^2(9\Lambda-7)}{(\Lambda+1)(81\Lambda^2-1)} \tag{2.22}$$

$$a_2 = (\Lambda-1)\left\{\frac{U_T(3)^2}{C_R^2} - \frac{16\Lambda^2}{(\Lambda+1)^2(9\Lambda-1)} + \frac{(\Lambda-1)(9\Lambda+1)}{(\Lambda+1)(9\Lambda-1)}\frac{U_T(1)^2}{C_R^2}\right\}$$

$$a_o = 2\frac{(\Lambda-1)^3}{(\Lambda+1)^2}\cdot\frac{(9\Lambda+1)}{(9\Lambda-1)}\frac{U_T(1)^2}{C_R^2}$$

Solutions are obtained by solving the sixth degree equation for $r(1)$ using numerical methods and searching for positive real roots only. In practice, the equation is solved as a cubic equation in $r(1)^2$. $r(3)$, $\delta(1)$ and $\delta(3)$ are then obtained from the first three expressions in (2.21). From the first equation it is seen that such solutions can be obtained only if $\Lambda > 1$. Since $r(3)^2$ shall be positive, it is also required that

$$r(1)^2 < 2\frac{\Lambda - 1}{\Lambda + 1} \tag{2.23}$$

This condition is used to limit the search for the roots in the cubic equation. In addition, we note from the expression for $\cos \delta(1)$ that the right hand side must be numerically less than 1.

The first problem was to determine the region of sloping waves in a region with the wavelength as abscissa and the total windshear as ordinate. This was done experimentally by solving the system (2.21), (2.22) for selected values of the two paramenters L and U_s. For a constant value of U_s the minimum and maximum value of L, for which the equations (2.21) have a solution, was determined. On the basis of these calculations Fig. 1 was constructed. It shows that non-sloping waves exist for sufficiently small wavelenghts for all values of U_s. For larger values of the wavelengths we find sloping waves for sufficiently large values of U_s. We can equally well say that the region of sloping waves, is the region of growing waves on the basis zonal current.

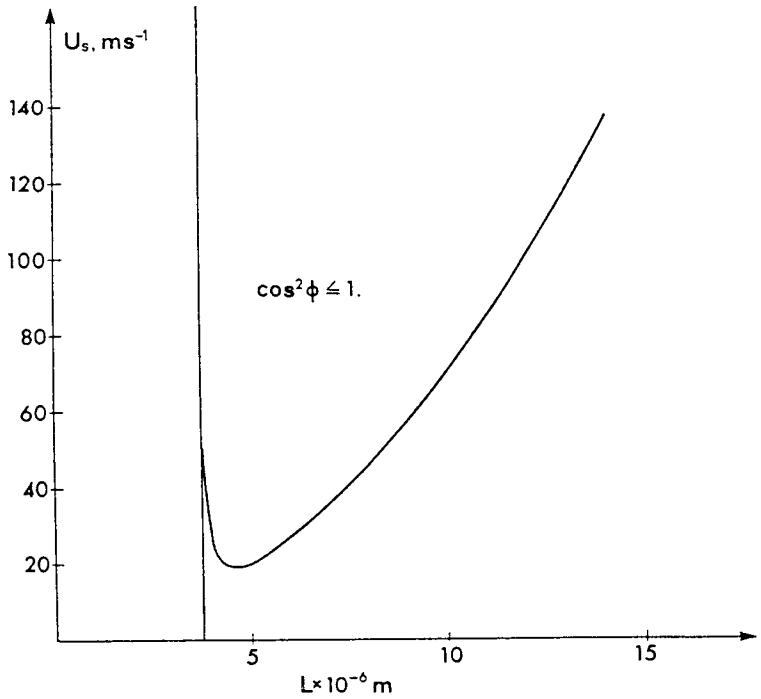

Fig. 1. The region marked $\cos^2 \Phi \leq 1$ is the values (U_s, L) giving sloping waves.

The structure of various waves is illustrated in Fig. 2 and Fig. 3. The upper part of Fig. 2 shows a case corresponding to summer conditions. We note the westward sloping wave with a total slope of only 40^0, while the relative amplitude increases from a very small value at the ground to substantial values at the top of the atmosphere. In the remaining figures we have used a value of $U_s = 40$ ms^{-1}, corresponding more to winter conditions. The value $l = 4$ ($L = 4000$

km) is close to the short wave cut-off. The vertical slope which is in general westward has the opposite slope in the middle of the atmosphere around $p_* = 0.5$. The slope is less complicated for somewhat longer waves as shown in Fig. 3. The resulting structures are thus qualitatively correct, but they are naturally influenced by the fact that we have included only two vertical components in the system. We may look at more complicated cases by integrating the time-dependent system (2.16) and (2.17) to the point where it arrives at a steady state. This has been done in a number of cases using more realistic wind profiles, and we shall show some results.

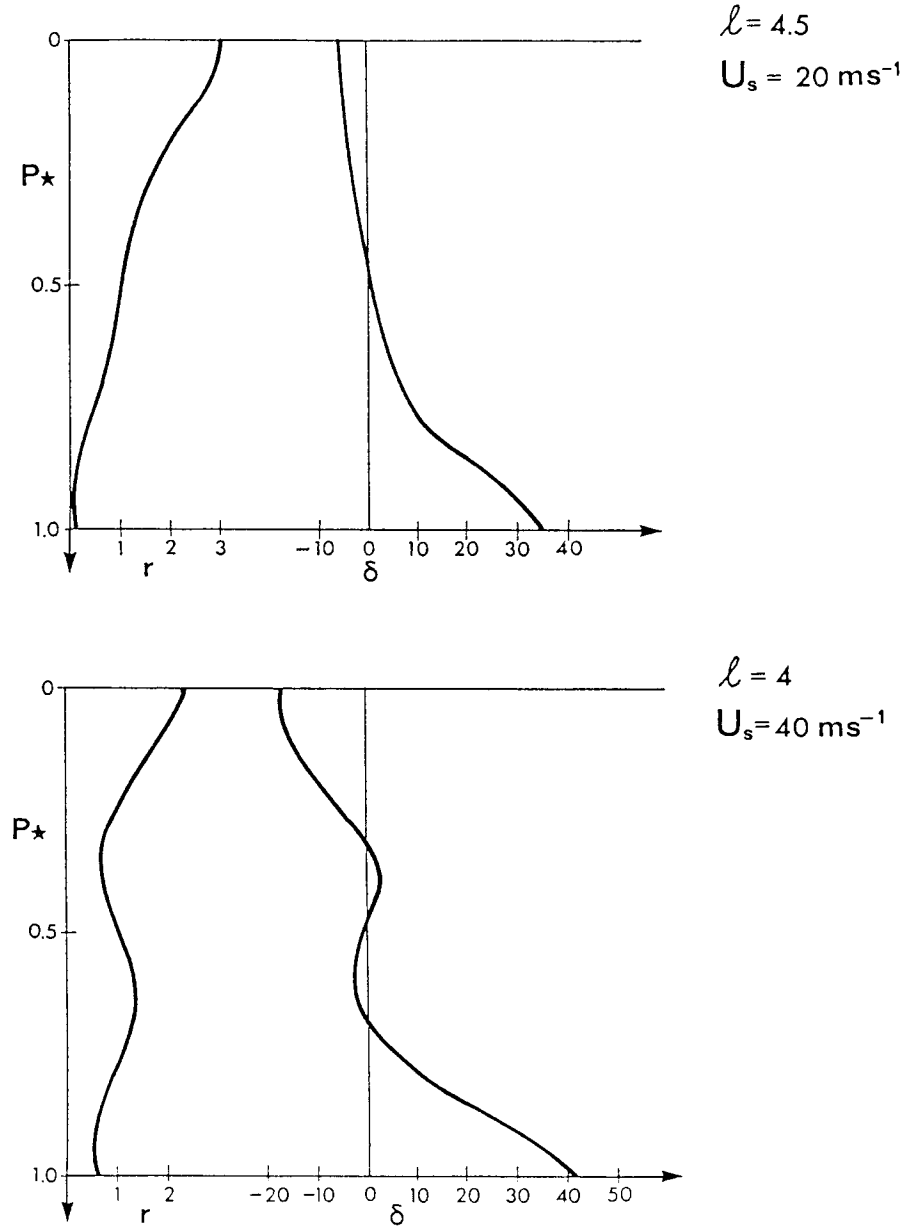

Fig. 2. The relative amplitude and the phase as a function of normalized pressure for $L = 4.5 \times 10^6$ m and $U_s = 20$ ms^{-1} and $L = 4 \times 10^6$ m and $U_s = 40$ ms^{-1}.

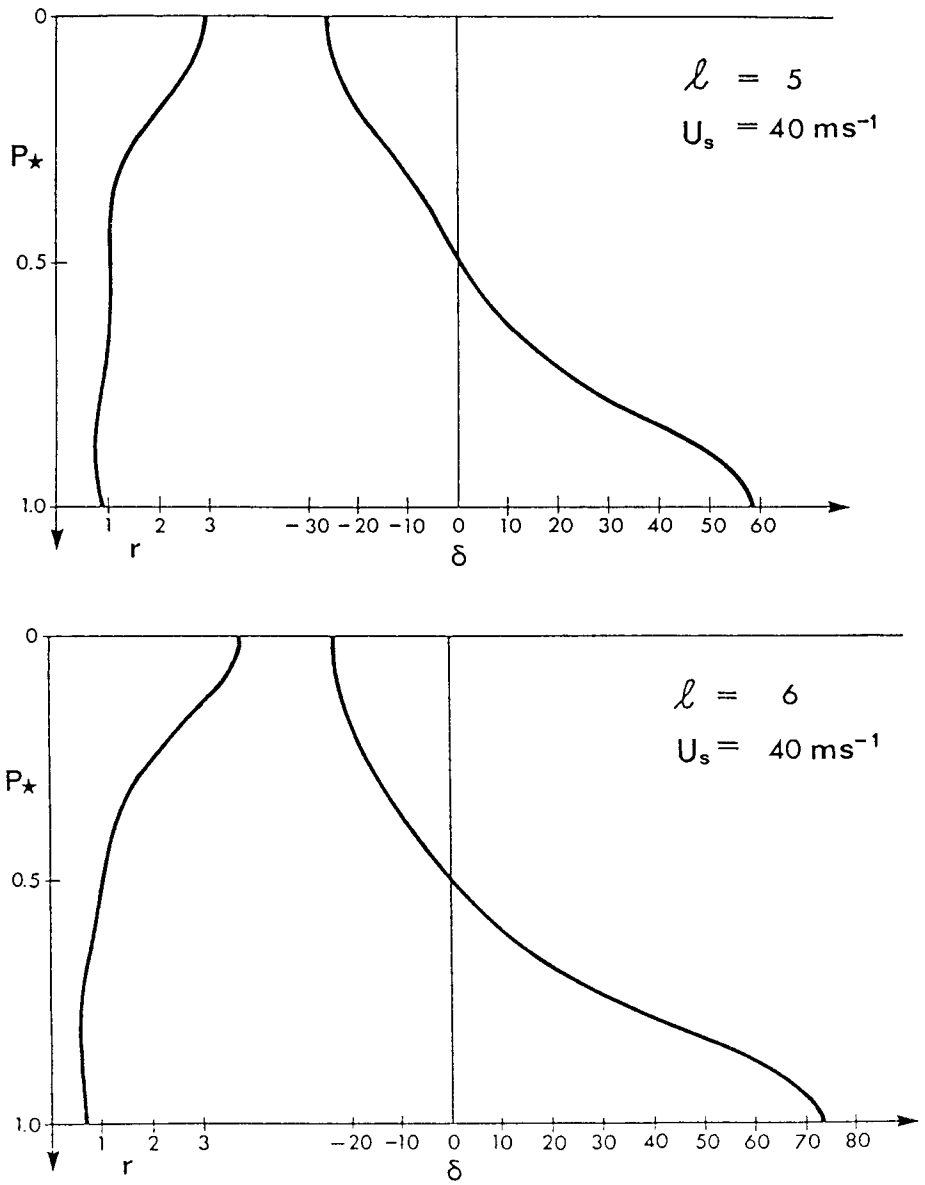

Fig. 3. As Fig. 2, but with $L = 5 \times 10^6$, $U_s = 40\text{ms}^{-1}$ (upper part) and $L = 6 \times 10^6\text{m}$, $U_s = 40\ \text{ms}^{-1}$ (lower part).

Fig. 4 shows the vertical profile of the zonal wind taken from Lorenz (1967) at 30°. The vertical mean wind has been removed from the data before plotting. We note the usual jet-maximum at about 25 kPa. This profile was used to calculate the Fourier coefficients for $U_s(p_*)$. The amplitude ratio $r(p_*)$, obtained after a steady state for the system (2.16), (2.17) has been reached, is shown in Fig. 5. There is a minimum at about 70 kPa in r, but the maximum in r is located close to the maximum in U_s. Note also the rapid decrease in r above the maximum, i.e. in the stratosphere. Fig. 6 shows the relative phase angle $\delta = \delta(p_*)$ for the same case. A westward slope is obtained from the ground to the level of the maximum wind, while an eastward slope is present in the stratosphere in good agreement with observations.

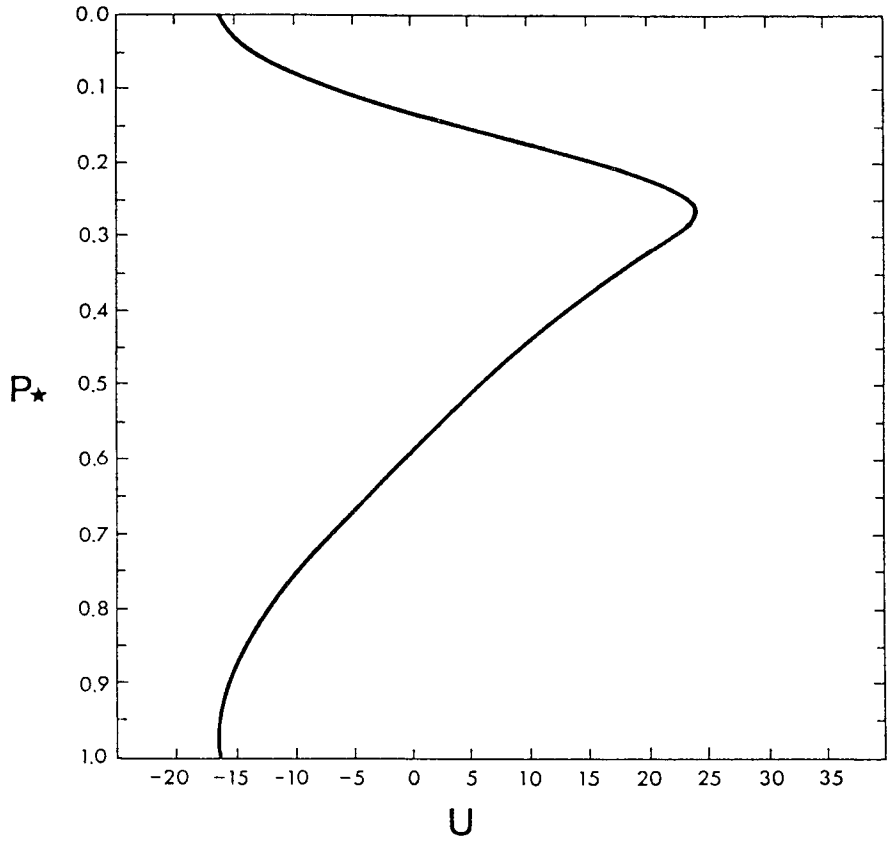

Fig. 4. $U = U(p_*)$ as obtained at 30°N from Lorenz (1967) . The vertical mean has been removed.

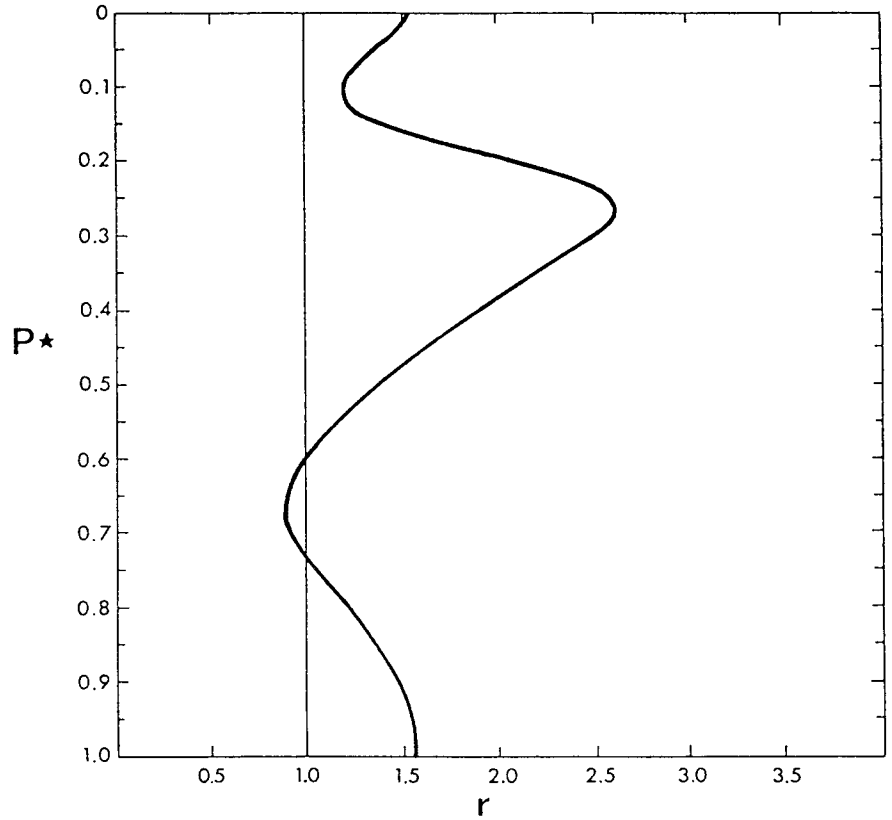

Fig. 5. The amplitude ratio, r, obtained as an asymptotic steady state for the wind profile in Fig. 4.

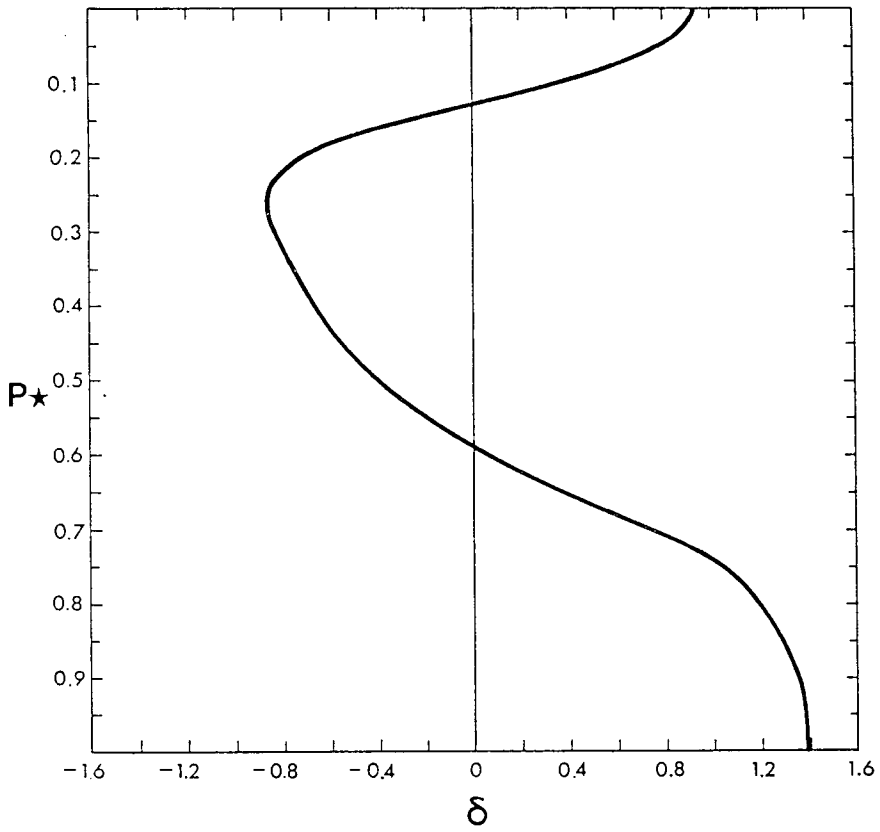

Fig. 6. The relative phase angle as a function of normalized pressure for the case in Fig. 4.

The sensitivity of the steady state for r and δ to the slope of the vertical wind profile is investigated in the following. For this purpose we use the following expression

$$U(p_*) = \frac{U_{\max}}{N(\alpha,\ \beta)} p_*^{\alpha}(1-p_*)^{\beta};\ \ N(\alpha,\ \beta) = \frac{\alpha^{\alpha}\beta^{\beta}}{(\alpha+\beta)^{\alpha+\beta}} \tag{2.24}$$

in which $\alpha \geq 1$, $\beta \geq 1$.

One may easily verify that the maximum wind occurs at the level $p_* = \alpha/(\alpha+\beta)$. As a first example we select a case in which the position of the maximum wind varies. For the four curves in Fig. 7 we have used $\alpha = 2$ and the following values of β:

Curve	A:	β=14,	p_*,max=0.125
"	B:	β=6,	p_*,max=0.25
"	C:	β=10/3,	p_*,max=0.375
"	D:	β=2,	p_*,max=0.5

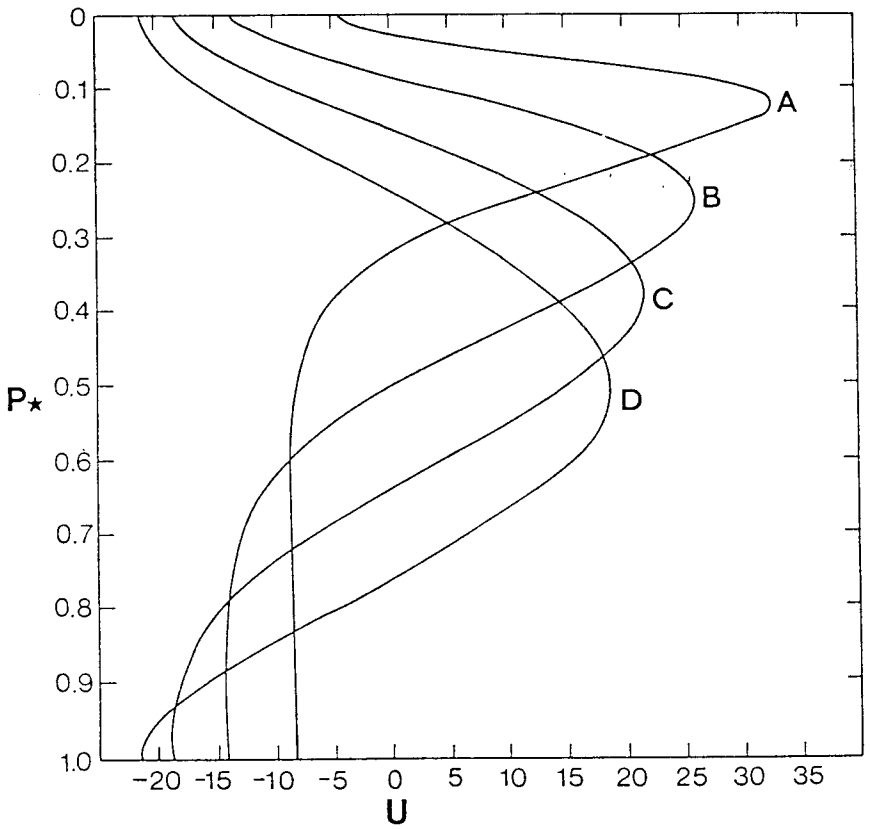

Fig. 7. Four vertical wind-profiles drawn using equation (5.24) . All four profiles have $\alpha = 2$ while β has the following values: A: $\beta = 14$; B:$\beta = 6$; C: $\beta = 10/3$ and D: $\beta = 2$.

The corresponding curves for $r = r(p_*)$ are shown (for curves A, B and C) in Fig. 8. It is seen that the maximum values of $r(p_*)$ is found at a lower value of p_* if the wind maximum occurs at lower values. Fig. 9 contains the corresponding curves for $\delta = \delta(r_*)$ showing a westward slope up to the wind maximum followed by a reversed slope along the wind maximum.

The sensitivity of the wave structure to the sharpness of the jet can be investigated by keeping the ratio α/β constant. We have used $\alpha/\beta = 1/3$ which results in p_*, max $= 0.25$. The profiles in Fig. 10 have $U_{\max} = 40$ ms^{-1} in all cases. Specifically, we have used:

Curve	A:	$\alpha = 2$,	$\beta = 6$
"	B:	$\alpha = 4$,	$\beta = 12$
"	C:	$\alpha = 6$,	$\beta = 18$
"	D:	$\alpha = 8$,	$\beta = 24$
"	E:	$\alpha = 10$,	$\beta = 30$

We get then an increasingly sharper jet as shown in Fig. 10. The amplitude ratio $r(p_*)$ is shown in Fig. 11. The maximum value of r occurs always at the same value of p_* as the wind maximum. The relative phase is shown in Fig. 12. Again we note the westward slope to the level of the wind maximum followed by the reserved slope above it.

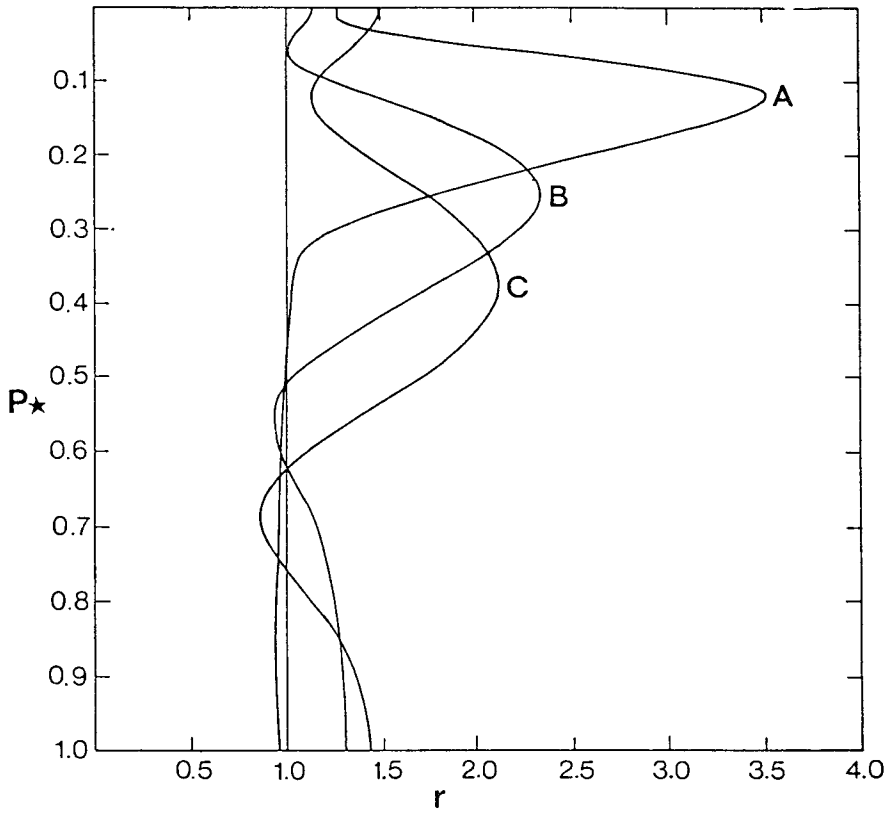

Fig. 8. The amplitude ratios for cases A, B and C.

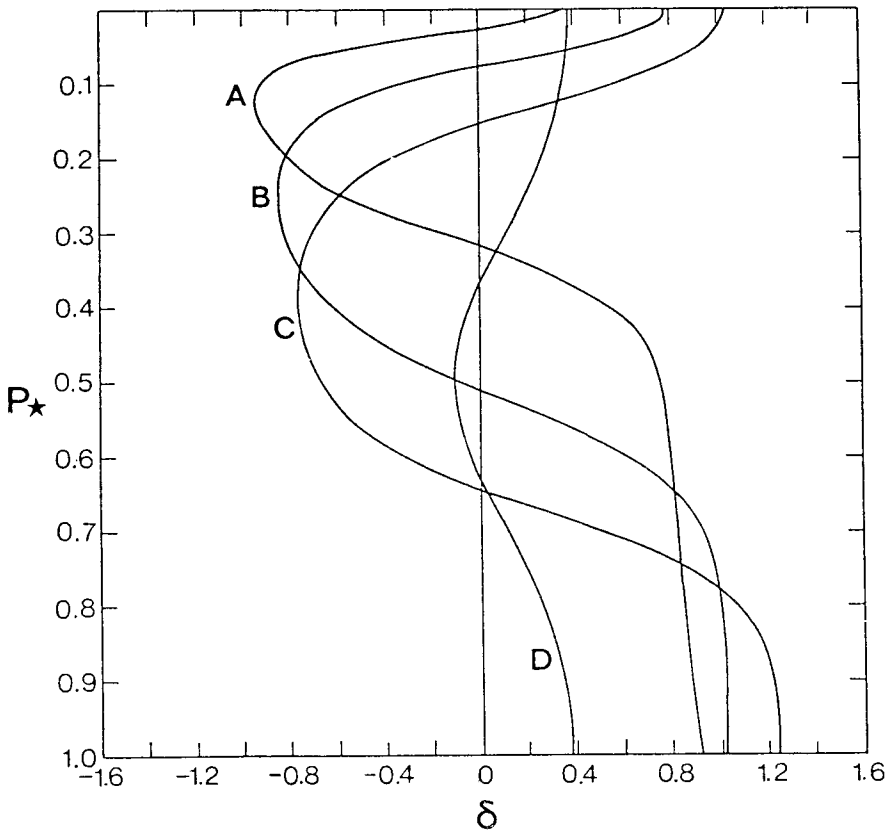

Fig. 9. The phase angles for cases A, B and D.

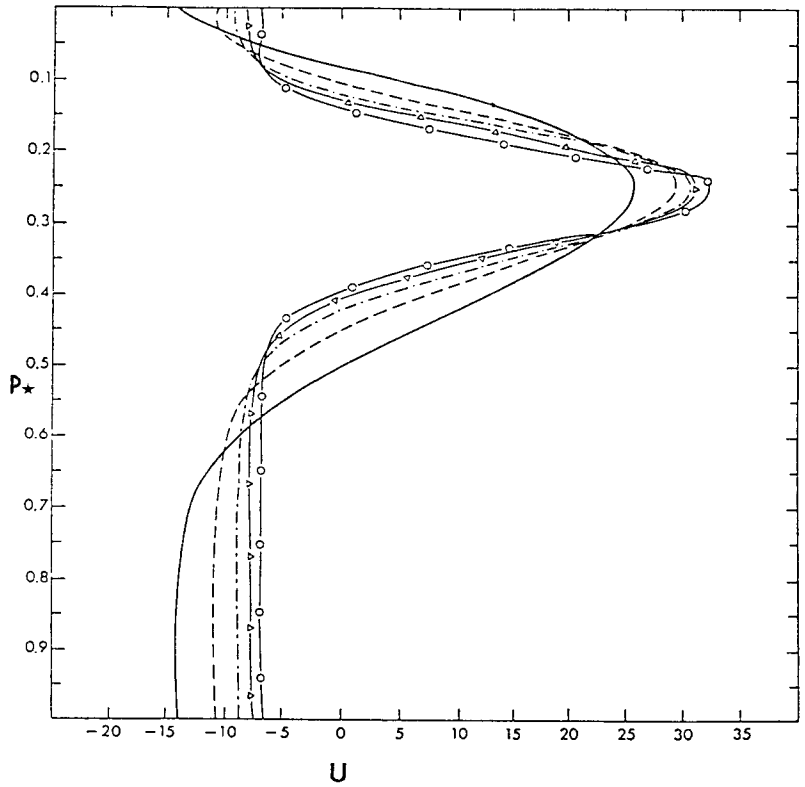

Fig. 10. Five vertical wind-profiles (eq. 5.24) having the same location of the maximum ($p_* = 1/4$). The values of α and β are: A: (2, 6); B: (4, 12) ; C: (6, 18); D: (8, 24); E: (10, 30).

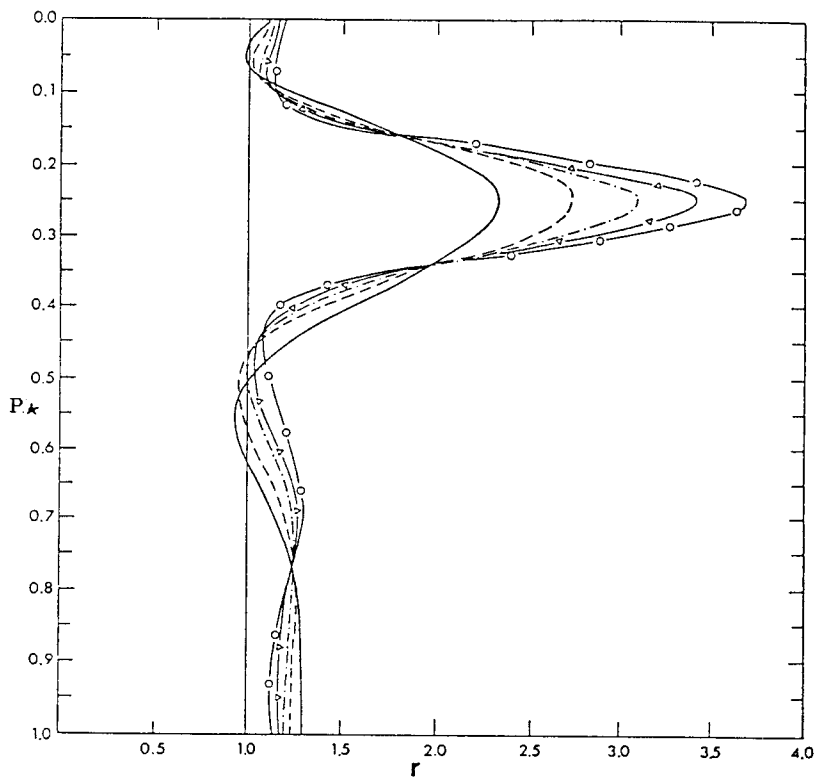

Fig. 11. The amplitude ratio for the five cases in Fig. 10.

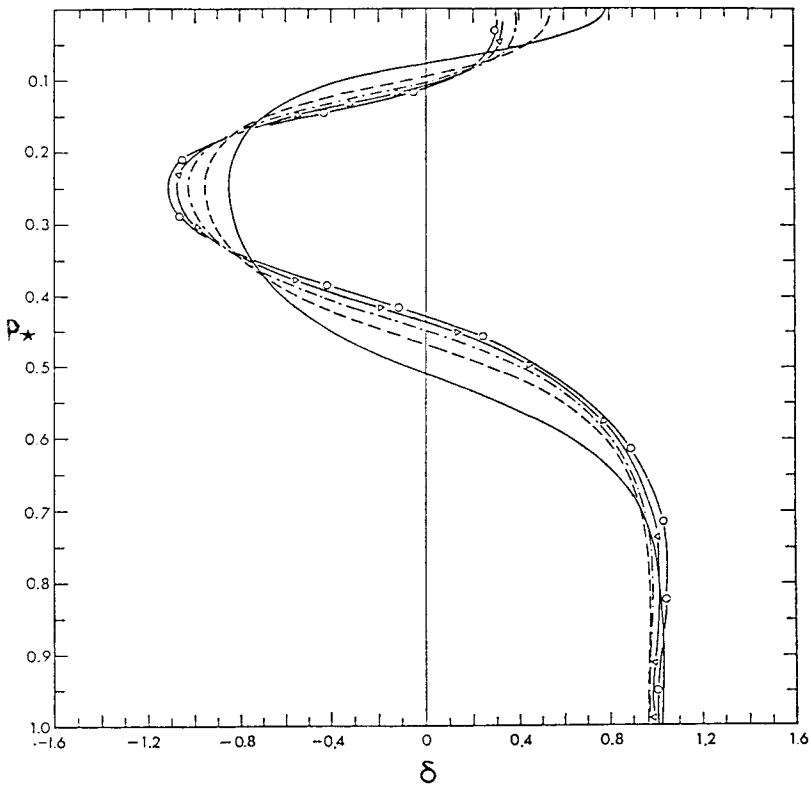

Fig. 12. The phase angles for the five cases in Fig. 10.

We may thus conclude that the relative structure of the wave is closely connected with the slope of the wind-profile in such a way that for a typical wind-profile with a maximum wind in the upper troposphere we obtain a westward tilt and an increase in the relative amplitude up to the wind maximum followed by a reversed slope and a decreasing amplitude above the maximum.

3. The vertical structure functions

The equation determining the vertical structure is well known (Wiin-Nielsen, 1971). We write it in the form

$$\frac{d}{dp^*}\left[\frac{fo^2}{\sigma po^2}\frac{dF}{dp_*}\right] + \lambda^2 F = 0 \tag{3.1}$$

for quasi-geostrophic motion. If σ were a constant we would get trigonometric functions as solutions. It is this case which is treated in Section 2.

According to Gates (1961) one may approximate the vertical variation σ by the expression:

$$\sigma = \frac{\sigma_o}{p_*^2} \tag{3.2}$$

where σ_o is the value of σ for $p_* = 1$ ($p = 100$ cb). We may try to find solutions to (3.1) with the

boundary conditions:

$$\frac{dF}{dp_*} = o \text{ for } p_* = p_T \text{ and } p_* = 1 \tag{3.3}$$

where p_T is a pressure level at which $\omega = 0$. Denoting

$$L_*^2 = \frac{\sigma_o p_o^2}{f_o^2} \tag{3.4}$$

we find that the following functions satisfy (3.1), (3.2) and (3.3)

$$G_n(p_*) = \frac{D(n)}{\sqrt{p_*}}\left[\sin\ (n\pi\frac{\xi}{\xi_T}) - 2\mu(n)\ \cos\ (n\pi\frac{\xi}{\xi_T})\right] \tag{3.5}$$

where

$$\mu(n)^2 = L_*^2\lambda^2(n) - \frac{1}{4} \tag{3.6}$$

giving

$$\lambda(n)^2 = \frac{1}{L_*^2}\left(\frac{1}{4} + \mu(n)^2\right) = \frac{1}{L_*^2}\left(\frac{1}{4} + \frac{n^2\pi^2}{\xi_T^2}\right) \tag{3.7}$$

We determine next $D(n)$ in such a way that

$$\int_{p_T}^{1} G_n(p_*)^2 dp_* = 1 \tag{3.8}$$

with the result that

$$D(n) = \left\{\frac{2}{(1 + 4\mu(n)^2)\xi_T}\right\}^{\frac{1}{2}} \tag{3.9}$$

The functions $G_n(p_*)$ form an orthogonal set because it is easy to show that

$$\int_{p_T}^{1} G_n(p_*)G_q(p_*)dp_* = \begin{cases} 1 & q=n \\ 0 & q\neq n \end{cases} \tag{3.10}$$

and it is also true that

$$\int_{p_T}^{1} G_n(p^*)dp^* = 0 \text{ for all } n \tag{3.11}$$

It is obvious that in this case it is a necessity to have $p_T > 0$. The model has thus a "lid" at a finite height. On the other hand, p_T can be as close to zero as one wants. From the definition of

the static stability parameter, i.e.

$$\sigma = -\alpha \frac{\partial ln\theta}{\partial p} = -\frac{R}{p}\left(\frac{\partial T}{\partial p} - \frac{R}{Cp}T\right) = \frac{\sigma_o p_o^2}{p^2} \tag{3.12}$$

one may solve for the temperature as a function of pressure. We find

$$T = T(p_*) = \frac{\sigma_o p_o^2 Cp}{R^2}(1 - p_*^{R/Cp}) + T_{op_*}^{R/Cp} \tag{3.13}$$

With the selected parameters T will vary from 283 K at the surface to 85.3 K at $p_* = 0$. The lapse rates connected with (3.13) vary from 0.7×10^{-2} km^{-1} at $p_* = 1$, 0.66 km^{-1} at $p_* = 0.5$, 0.60 km^{-1} at $p_* = 0.2$ to 0 at $p_* = 0$. This model atmosphere is thus isothermal at the top.

As will be seen in the next section it will be required to evaluate interaction coefficients which will be defined by the integral

$$I(q,\ r,\ s) = \int_{p_T}^{1} G_q(p_*)G_r(p_*)G_s(p_*)dp_* \tag{3.15}$$

For the evaluation of (3.15) there are several posibilities. The functions $G_n(p_*)$ defined by (3.5) are so elementary that it is possible to carry out the integration in (3.15) directly, and this is the method used in the following section, but one could just as well use one of the standard numerical integration formulas.

The specification (3.2) of the dependence of the static stability parameter on pressure is not the only possibility. Jacobs and Wiin-Nielsen (1966) have solved the same equation for the case where the thermal stratification is given by a constant lapse-rate. In this case one obtains

$$\sigma = \frac{\sigma_o}{p_*^{2-R\gamma/g}} \tag{3.16}$$

with

$$\sigma_o = \frac{R^2 T_o}{g p_o^2}(\gamma_d - \gamma) \tag{3.17}$$

For a standard value of $\gamma = 6.5 \times 10^{-3}$ km^{-1} we find that the exponent in the denominator of (3.16) has the values 1.8 which differs from the one in (3.2) by only 10%. The solutions are in this case Bessel Functions which may be written in the form

$$F = \text{const. } \xi^{-n} J_n(2(n+1)\lambda(n)\xi) \tag{3.18}$$

where

$$n = \frac{g}{R\gamma} - 1 \tag{3.19}$$

and

$$\xi = p_*^{\frac{1}{2(n+1)}} \tag{3.20}$$

The boundary condition dF/dp_* at $\xi = 0$, $\xi = 1$ results in the expression

$$J_{n+1}[2(n+1)\lambda(n)] = 0 \tag{3.21}$$

which means that the values of $\lambda(n)$ are determined by the zeroes of the Bessel function of order $(n+1)$. The value of n is determined from (3.19). It is of course an advantage to work with integer values of n. For $n = 4$ we find a value of $\gamma = 6.8 \times 10^{-3}$ km^{-1}.

For the functions (3.21) there is an orthogonality condition which according to Abramowitz and Stegun (1964) is

$$\int_0^1 \xi J_n(2(n+1)\lambda_i\xi) J_n(2(n+1)\lambda_j\xi) d\xi = \begin{cases} 0 & i \neq j \\ \frac{1}{2}[J_n(2(n+1)\lambda_i)]^2 & i = j \end{cases} \tag{3.22}$$

It is thus seen that this family of Bessel functions can be used also as vertical structure functions. We note especially that the functions (3.18) are well behaved for $\xi \to 0$ because for small values of the argument we have

$$J_n(2(n+1)\lambda_i\xi) \simeq \frac{1}{2^n} \cdot \frac{1}{n} [2(n+1)\lambda_i\xi]^n \tag{3.23}$$

and therefore

$$\xi^{-n} J_n(2(n+1)\lambda_i\xi) \simeq \frac{1}{2^n} \frac{1}{n} [2(n+1)\lambda_i]^n \tag{3.24}$$

In addition, they satisfy the upper boundary condition automatically because

$$\frac{d}{d\xi}\left[\xi^{-n} J_n[2(n+1)\lambda_i\xi]\right] = -2(n+1)\lambda_i \xi^{-n} J_{n+1}[2(n+1)\lambda_i\xi] \tag{3.25}$$

and the right side of (3.25) goes to zero according to (3.23) as ξ approaches zero.

In the present paper we shall limit ourselves to the functions (3.5), but we hope at a later occasion to use the functions (3.18).

We finish this section with some comments on the boundary conditions. If we were to replace the lower boundary condition with $w = dz/dt$ we would obtain

$$g\frac{dz}{dt} = \frac{\partial\phi}{\partial t} + \vec{V} \cdot \nabla\phi + \omega\frac{\partial\phi}{\partial p} \simeq (\frac{\partial\phi}{\partial t})_o - \frac{RT_o}{p_o}\omega_o = 0, \quad p = p_o \tag{3.26}$$

leading to

$$\omega_o = \frac{p_o f_o}{RT_o}(\frac{\partial\psi}{\partial t})_o \tag{3.27}$$

The thermodynamic equation employed at $p = p_o$ is then

$$\frac{\partial}{\partial t}\left[\frac{f_o}{\sigma_o}(\frac{\partial \psi}{\partial p})_o\right] + \vec{V} \cdot \nabla\left[\frac{f_o}{\sigma_o}(\frac{\partial \psi}{\partial p})_o\right] + \frac{p_o f_o}{RT_o}(\frac{\partial \psi}{\partial t})_o = 0, \ p = p_o \tag{3.28}$$

but since the vertical structure functions apply to a resting atmosphere it follows from (3.28) that at the lower boundary we have

$$\frac{dG}{dp_*} + \frac{\sigma_o p_o^2}{RT_o} G = 0, \ p = p_o \tag{3.29}$$

where

$$r = \frac{\sigma_o p_o^2}{RT_o} \simeq 0.11 \tag{3.30}$$

The basic equation (3.1) and its general solution are still the same, but the integration constants will have new values in view of (3.29). For the case of $\sigma = \bar{\sigma} = \sigma_o = \text{const.}$, treated in section 2, we find that $\mu(n) = n\Pi$ are replaced by the solutions to the transcendental equation

$$\mu \tan [(1 - p_T)\mu] = r \tag{3.31}$$

The roots of (3.31) are obtained numerically. The following Table 1 contains the new and the old values of μ

Table 1 ($\bar{\sigma} = \text{const.}$)

n	μ(n), new	μ(n), old
0	0.3257	-
1	3.1762	3.1416
2	6.3006	6.2832
3	9.4364	9.4248
4	12.5751	12.5664
5	15.7150	15.7080
6	18.8554	18.8496
7	21.9962	21.9911

It is thus seen that in the case of constant σ the values of $\mu(n)$ do not deviate very much from each other except for the basic mode ($n = 0$) which exists only with the new boundary condition. We conclude that the structures will not change radically.

We turn next to the case where σ's variation with γ is given by (3.2). Considering first the external mode we find a solution to (3.1) which is

$$F(p_*) = C_1 P_*^{\mu_o - \frac{1}{2}} + C_2 p_*^{-\mu - \frac{1}{2}}, \ \mu_o^2 = \frac{1}{4} - L_*^2 \lambda_o \tag{3.32}$$

Applying the boundary condition (3.29) at $p_* = 1$ and $dF/dp_* = 0$ at $p_* = p_T$ we find that μ,

is determined by the equation

$$\tanh\ (\xi_T \mu_o) + \frac{4r\mu_o}{4\mu_o^2 - 1 + 2r} = 0 \tag{3.33}$$

which has only one solution found by numerical methods to be

$$\mu_o = 0.369.$$

Finally, applying the same boundary conditions to the internal solutions it turns out that the equation for $\mu(n)$ is

$$\tanh\ (\xi_T \mu(n)) = \frac{4r\mu(n)}{4\mu(n)^2 + 1 - 2r} \tag{3.34}$$

The solutions can also in this case be found by standard root finding routines. We give the results in Table 2.

Table 2 ($\bar{\sigma} = \sigma_o p_*^{-2}$)

n	μ(n), new	μ(n), old = nΠ/ξ_T
0	0.369	0
1	1.395	1.364
2	2.746	2.729
3	4.105	4.093
4	5.466	5.458
5	6.829	6.822
6	8.192	8.186
7	9.556	9.551

We conclude also in this case that the two sets of values are sufficiently close to prevent major changes in the structure of the waves. This result is explained by the small value of r. With the adopted value of r we find that the function on the right hand side of (3.34) is zero at $\mu(n) = 0$, has a maximum of 0.12 at $\mu = 0.44$ and goes to zero as μ goes to infinity. With this shape it is clear that the intersections of this curve with the various branches of the tanh-function must be close to the zeroes of this function, and it is of course the position of these zeroes which determine the values in the third volume of Table 2.

4. A model with variable static stability

As mentioned in Section 4 we shall formulate a model based on a vertical variation of the static stability parameter according to (3.2) resulting in the vertical structure functions (3.5). In the formulation of the governing equations we make repeated use of (3.1). We assume from the beginning that the zonal wind $U_T(p)$, which is defined as the deviation of the wind profile $U(p)$

from its vertical mean U_M, is given in the form

$$U_T(p_*) = \sum_{n=1}^{\infty} U_T(n) G_n(p_*) \tag{4.1}$$

The components $U_T(n)$ are calculated by the integrals

$$U_T(n) = \int_{p_T}^{1} U_T(p_*) G_n(p_*) dp_* \tag{4.2}$$

For the streamfunction $\psi'(x,\ t,\ p_*)$ we assume in a similar way:

$$\psi'(x,\ t,\ p_*) = \sum_{n=1}^{\infty} (A(n,\ t)\ \cos\ kx + B(n,\ t)\ \sin\ kx) G_n(p_*) \tag{4.3}$$

where we shall follow the same methodology as in Section 2 meaning that

$$A(n,\ t) = R(n,\ t)\ \cos\ \theta(n,\ t);\ \ B(n,\ t) = R(n,\ t)\ \sin\ \theta(n,\ t) \tag{4.4}$$

and that

$$r(n,\ t) = \frac{R_T(n,\ t)}{R_M(t)};\ \ \delta(n,\ t) = \theta_M(T) - \theta_T(n,\ t) \tag{4.5}$$

With these reminders we need to state only that the final equations are obtained using exactly the same procedures as in Section 2. We write the final equations in the form:

$$\frac{dr(n)}{dt} = -k\Bigg[\frac{1-\lambda(n)^2}{1+\lambda(n)^2} U_t(n)\ \sin\ \delta(n) + \sum_{s=1}^{N} U_T(\delta) r(n)\ \sin\ \delta(s)$$

$$+ \sum_{s=1}^{N}\sum_{l=1}^{N}\Bigg[\frac{1+\lambda(1)^2-\lambda(s)^2}{1+\lambda(n)^2} I(n,\ s,\ l) U_T(s) r(l)\ \sin\ (\delta(n) - \delta(l))\Bigg]\Bigg]$$

$$\frac{d\delta(n)}{dt} = -k\Bigg[\frac{1-\lambda(n)^2}{1+\lambda(n)^2}\frac{U_T(n)}{r(n)}\ \cos\ \delta(n) - \sum_{s=1}^{N} U_T(s) r(s)\ \cos\ \delta(s)$$

$$+ \sum_{s=1}^{N}\sum_{l=1}^{N}\Bigg[\frac{1+\lambda(l)^2-\lambda(s)^2}{1+\lambda(n)^2} I(n,\ s,\ l) U_T(s)\frac{R(l)}{R(n)}\ \cos\ (\delta(n) - \delta(1))\Bigg]$$

$$+ \frac{\lambda(n)^2}{1+\lambda(n)^2} C_R\Bigg] \tag{4.6}$$

where $\lambda(n)$ is given by (3.7), and where

$$I(n,\ s,\ l) = \int_{p_T}^{1} G_n(p_*)G_s(p_*)G_l(p_*)dp_* \tag{4.7}$$

An inspection of the system (4.6) shows clearly that a direct determination of the steady states is not very likely. With the experience from the previous cases, especially Section 2 in this paper, but also I and II, we may hope to obtain asymptotic steady states by integrating the system (4.6) in time using a suitable time-integration scheme. Such an asymptotic steady state may or may not be obtained by such a procedure. It may for example happen that the solution is of an oscillatory nature in which case no time-independent asymptotic solution is obtained.

The time-integration scheme has been Heun's scheme which for a single equation

$$\frac{dx}{dt} = F(x) \tag{4.8}$$

consists of computing a preliminary estimate

$$x^* = x(n) + \Delta t \cdot F(x(n)) \tag{4.9}$$

while the final estimate is

$$x(n+1) = x(n) + \frac{1}{2}\Delta t(F(x(n)) + F(x^*)) \tag{4.10}$$

The application of the numerical scheme to the system (4.6) is straightforward.

The next question which will be considered is the vertical resolution necessary to resolve a given wind-profile. For traditional reasons it is perhaps pertinent to consider first a linear profile for $U_T(p_*)$, say

$$\frac{U(p_*)}{U_T} = \frac{\frac{1}{2}(1+p_T) - p_*}{1-p_T} \tag{4.11}$$

For $p_T = 0.1(\sim 10$ kPa) we find the values of $U(n)$ listed in Table 3.

Table 3

n	1	2	3	4	5	6	7	8	9	10
U(n)	0.2440	0.1017	0.05580	0.03117	0.02184	0.01445	0.01141	0.008252	0.006976	0.005318

From the values shown in Table 3 we may regenerate $U(p^*)$ from the original formula (4.1). The

result is shown in Fig. 13 which shows a good fit to the straight line except close to $p_* = p_T = 0.1$ and $p_* = 1$. It is obvious that there will always be such a deviation because at the boundaries $dF/dp_* = 0$ while the straight line does not satisfy this condition.

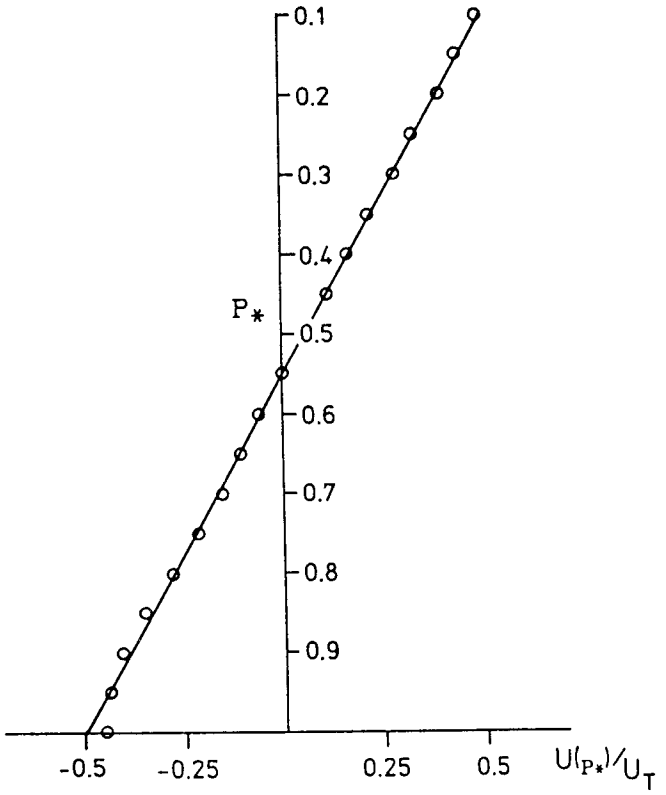

Fig. 13. The circles are obtained by adding the contributions from 10 components as an approximation to the linear windprofile.

We may try next with a profile which does satisfy the conditions of a vanishing derivative for $p_* = p_T$ and $p_* = 1$. For this purpose we design a wind-profile with a vanishing vertical mean and a maximum U_m at a certain pressure level p_m. The resulting wind-profile is a modification of the one given in (2.24) from which we have removed the vertical mean. The result is

$$U_T(p_*) = \frac{U_m}{\frac{\alpha^\alpha \beta^\beta}{(\alpha+\beta)^{\alpha+\beta}} - \frac{\alpha!\beta!}{(\alpha+\beta+1)!}} \cdot \left[\frac{(p_* - p_T)^\alpha (1-p_*)^\beta}{(1-p_T)^{\alpha+\beta}} - \frac{\alpha!\beta!}{(\alpha+\beta+1)!} \right] \tag{4.12}$$

A case with $\alpha = 3$, $\beta = 9$ was selected. For the following figure we have also taken $p_T = 0$. The comparison between (4.12) (full curve) and the recomputed windprofile using 10 components (circles) is shown in Fig. 14. The maximum deviation occurring at the wind maximum is 3%. It would thus seem that about 10 components are sufficient to approximate the windprofiles, but there is of course no guarantee that this number of components will suffice also for the wave structure, since this will depend on the computed steady state, and on how fast the components of the relative amplitude decrease as the vertical wave number increases. Only the results will show.

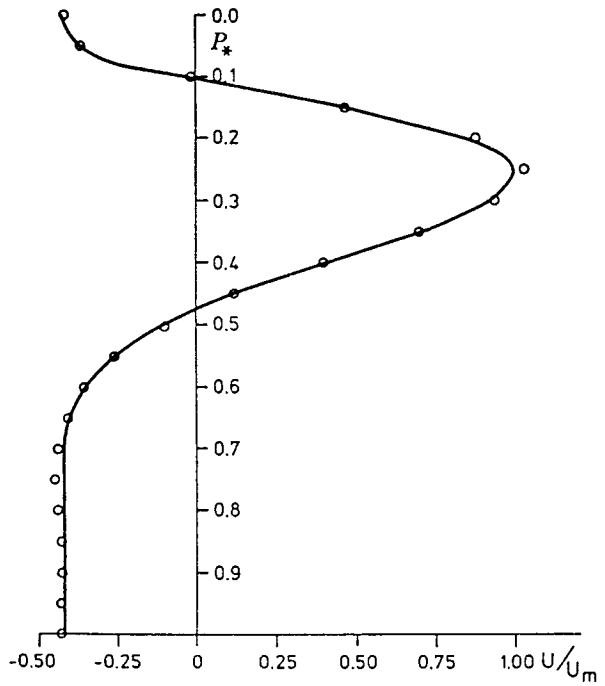

Fig. 14. Similar to Fig. 13, but for the jet stream profile.

We return to the integration of the system (4.6) using Heun's numerical time-integration scheme. To carry out a single integration it is necessary to specify the wavelength L and the profile of the wind in the basic state given by the components $U(n)$; $n = 1, 2, ..., N$. For the linear profile (4.11) it is seen that the coefficients $U(n)$ are proportional to U_T. For a given value of U_T which is the total windshear from $p_* = 1$ to $p_* = p_T$, we obtain the coefficients $U(n)$ by multiplying the values in Table 3 by U_T. It is thus natural to present the results in a (L, U_T)-diagram. The total calculation has therefore consisted of a large number of separate calculations, each corresponding to a point in the (L, U_T)-plane. For each time-integration we define a convergence criterion. It is

$$| r(n+1) - r(n) | < \epsilon \text{ and } | \delta(n+1) - \delta(n) | < \epsilon \text{ for all } n \tag{4.13}$$

where ϵ is a small number, normally set to 10^{-6}.

If convergence is obtained, we have as a result an asymptotic, stable, steady state characterized by the two sets: $r_s(n)$ and $\delta_s(n)$. Assuming that $\theta_M = 0$ and thus $R_M = A_M$ we find that

$$a(p^*) = 1 + \sum_{n=1}^{N} r(n) \cos \delta(n) \cdot G_n(p^*)$$

$$b(p^*) = -\sum_{n=1}^{N} r(n) \sin \delta(n) \cdot G_n(p^*) \tag{4.14}$$

From (4.14) we may then compute amplitude and phase angle in the usual way. These two quantities will be used to illustrate the wave structure.

It turns out as one would expect that the results in this case are quite similar to those presented in Section 2. The reason is that the new vertical structure functions are modified forms of the trigonometric cos-function used in the earlier section. Since the figures, given earlier, illustrates the structures quite well, we shall be satisfied by giving a couple of examples. Fig. 15 shows the relative amplitude and phase for a case when the wavelength is 4000 km and the total windshear 90 ms^{-1}. The maximum amplitude occurs at a lower level in the atmosphere than in Section 2, and, while the wave is still sloping westward, there is a reversed slope in the upper level. Both of

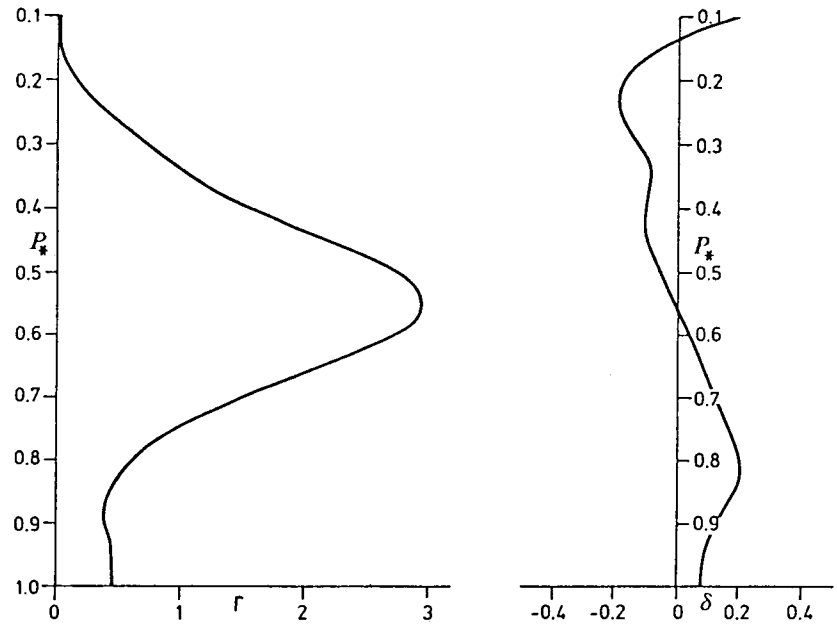

Fig. 15. The relative amplitude and phase for a wavelength of 4000 km and a maximum speed of 90 ms^{-1} in the basic current.

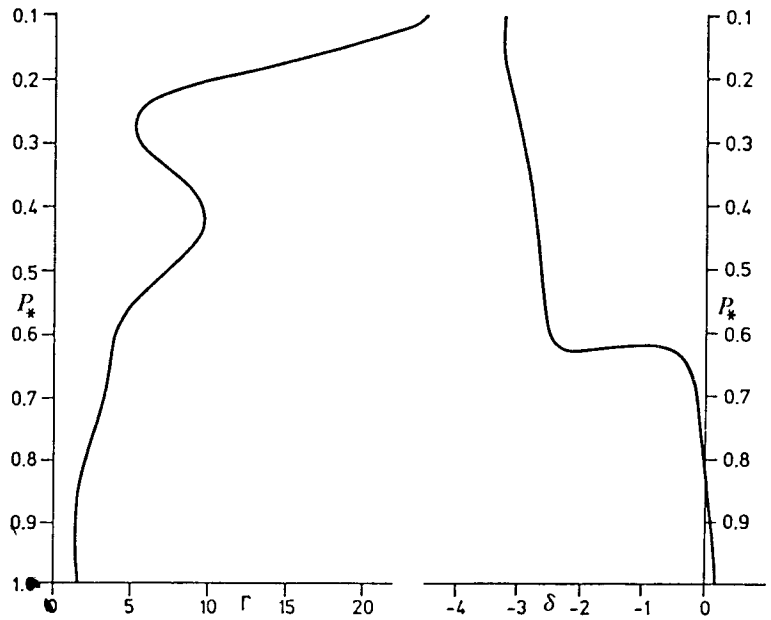

Fig. 16. The relative amplitude and phase for a wavelength of 11000 km and a maximum speed of 50 ms^{-1} in the basic current.

these features are presumably due to the increase of the static stability with height, while, as we recall, the stability parameter was constant in the case treated in Section 2.

Fig. 16 shows an extreme case where the wavelength is 11000 km and the total windshear 50 ms^{-1}. As we shall see later this wave is only very slightly unstable (Its e-folding time is 10 days). It has a very large increase of the relative amplitude with height, containing two maxima. The slope is only very slightly westward in a lower and a higher section with a very rapid transition around 60 kPa. The total slope is about half a wavelength. The structure, presented in Fig. 16, is typical of all the structures where the instability is very slight, i.e. very small growth rates. This feature makes the waves rather uninteresting.

Fig. 17 and Fig. 18 have been prepared in such a way that they are directly comparable to the two parts of Fig. 3. This has been accomplished by including the same components in the two cases. We notice that the vertical variation of the static stability parameter makes quite a difference. The larger values in the upper part of the atmosphere of σ removes the maximum relative amplitude from the upper boundary, and it is now found at a level of about $p_* = 0.2$. The total slope has also become smaller, and there is in Fig. 17 a reversal of the slope close to the upper boundary.

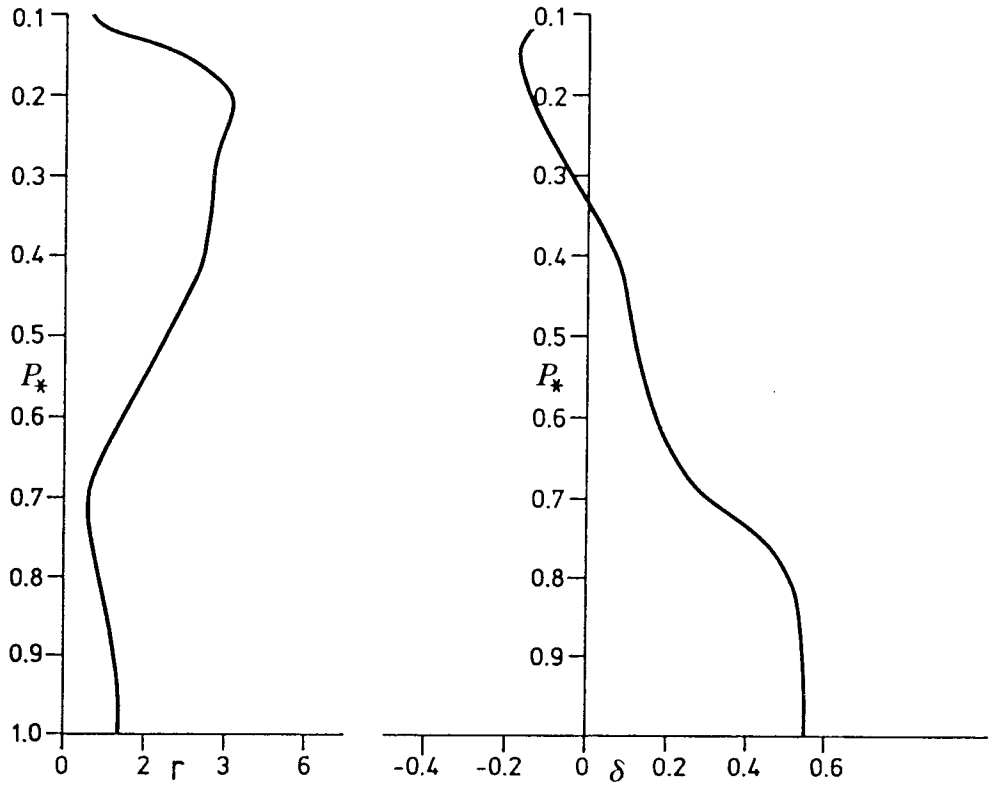

Fig. 17. Relative amplitude and phase $L = 5000$ km, $U_T = 40$ ms^{-1}. Only 3 vertical components.

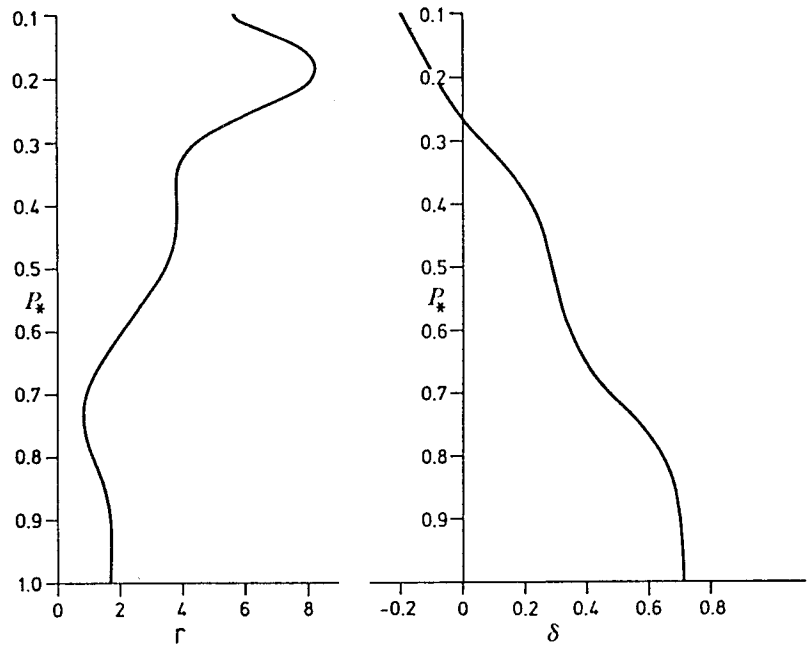

Fig. 18. Relative amplitude and phase. $L = 6000$ km, $U_T = 40$ ms^{-1}. Only 3 vertical components.

Although the first purpose of this investigation is to determine the relative structure of transient waves it turns out that the procedure of finding the stable steady states for $r = R_T/R_M$ and $\delta = \theta_M - \theta_T$ actually permits a determination of the growth rate and the phase speed for the sloping waves which are the baroclinically unestable waves. We start by recalling that in a steady state we have $dr/dt = 0$ and $d\delta/dt = 0$. From the first condition and the definition of r it follows that

$$R_M \frac{dR_T}{dt} - R_T \frac{dR_M}{dt} = 0 \tag{4.15}$$

or

$$\frac{1}{R_T}\frac{dR_T}{dt} = \frac{1}{R_M}\frac{dR_M}{dt} \tag{4.16}$$

On the other hand, if we were to make a standard stability analysis we would assume that

$$\psi_M = \hat{\psi}_M e^{ik(x-ct)} \tag{4.17}$$

from which we would get

$$R_M = e^{kc_i t}(\psi_{Mr}^2 + \psi_{Mi}^2)^{\frac{1}{2}} \tag{4.18}$$

or

$$\frac{dR_M}{dt} = kc_i R_M \tag{4.19}$$

It follows then that

$$kc_i = \frac{1}{R_M}\frac{dR_M}{dt} = k\sum_n U_T(n)r(n)\ \sin\ (\delta(n)) \tag{4.20}$$

where the last expression is obtained from an equation for dR_M/dt. We write finally

$$c_i = \sum_{n=1}^{N} U_T(n)r_s(n)\ \sin\ \delta_s(n) \tag{4.21}$$

where the subscript s indicates that (4.21) is valid in the steady state only. For the phase angles we have in the steady state

$$\frac{d\delta}{dt} = \frac{d\theta_M}{dt} - \frac{d\theta_T}{dt} = 0 \tag{4.22}$$

and calculating the phase angle from (4.17) we find

$$-\theta_M = -kc_r t \tag{4.23}$$

and, consequently,

$$\frac{d\theta_M}{dt} = kc_r \tag{4.24}$$

giving

$$c_r = \frac{1}{k}\frac{d\theta_M}{dt} \tag{4.25}$$

and, from the equation for $d\theta_M/dt$, the final result

$$C_r - U_M = -c_R + \sum_{n=1}^{N} U_T(n)r_s(n)\ \cos\ \delta_s(n) \tag{4.26}$$

Finally, the e-folding time T_e can be obtained from

$$T_e = (kc_i)^{-1} \tag{4.27}$$

We shall make use of (4.21) and (4.26) to find c_i and c_r. This numerical method to determine the real and imaginary part of the phase speed is new. It is similar to the method employed by Brown (1969) because he performs a time-integration of the linear pertubation equations in a two-dimensional grid, but he does not make use of the relative amplitude and the relative phase. The method contains also some similarities to the investigation of Kasahara and Tanaka (1989) because they make use of vertical structure functions in much the same way as this study. On the other hand, their solution of the eigen-value problem uses a matrix method, and the structure functions employed by them satisfy a more general boundary condition at the lower boundary than the condition $\omega = 0$ employed in this study.

The advantage of the method in this investigation is that the structure and the phase speed can be obtained directly once the steady state solution to the system (4.6) has been obtained. On the other hand, the steady state solution may require extensive calculations unless the initial guess, i.e. the starting position, is close to the steady state. In this study we have employed the technique of solving the system (4.6) in a two-dimensional grid with coordinates (L, U_s) where L is the wavelength and U_s is a measure of the vertical shear. It turns out that the convergence is most rapid when the instability is large. The first point in which a calculation is attempted should thus in general have a large windshear and a moderately small wavelength. When the solution has been obtained in the first point, it may be used as the initial condition for the solution in a neighboring point. It pays as a matter of fact to obtain all solutions for a given L, i.e. a vertical column in the diagram. Each of these solutions can then be used to generate the solutions in the horizontal rows.

While the method used here may be new it cannot give results different from those already obtained by other methods. We shall therefore restrict ourselves to some examples. As a first example we take the wind-profile shown in Fig. 13 in which 10 components $U(n)$ were used. This profile is of course an approximation to a linear increase of the basic current, but it is not indentical to the linear wind-profile. As a matter of fact, the linear wind-profile cannot be obtained in the limit of infinitely many structure functions because all structure functions have zero-derivatives at the two boundaries, while this is not the case for the linear wind-profile.

Fig. 19 shows the most important aspects of the stability diagram. The curves show the growth rate in the unit: days^{-1}. The lower curve is the neutral stability curve. No attempt has been made to map the weak instability for very long waves. Fig. 20 contains the isolines for $U_M - c_r$ in ms^{-1}. The isolines are in both cases restricted to the region $L \geq 1000$ km. Thus no attempt has been made to determine whether or not a short-wave cut-off is present. This problem as well as the very long wave weak instability have been disregarded since they are treated in detail in many other investigations as for instance Kasahara and Tanaka (1989) and Green (1960).

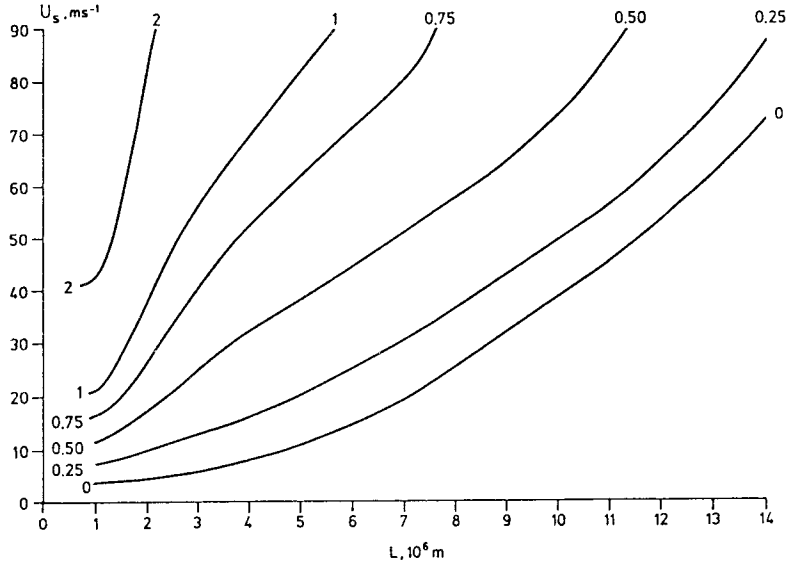

Fig. 19. The growth rate (days^{-1}) for a linear basic wind-profile approximated by 10 vertical components in a diagram with wavelength and maximal windshear along the horizontal and vertical axes.

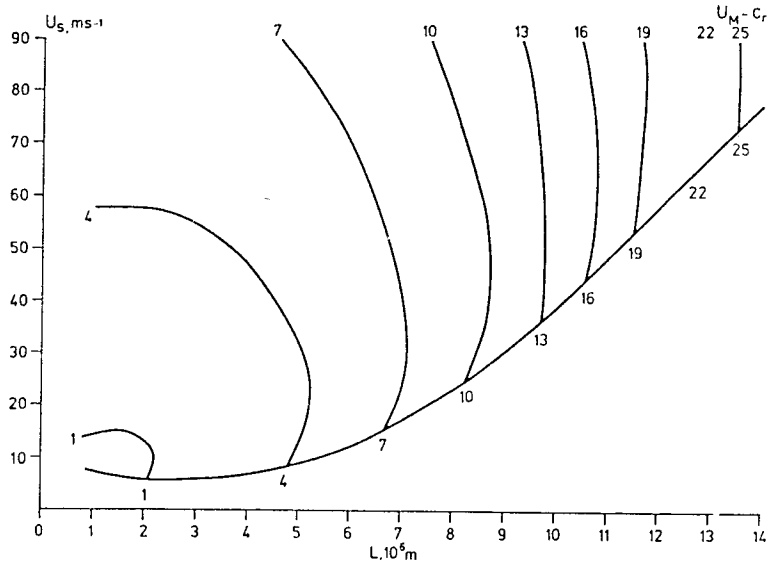

Fig. 20. A measure of the phase speed $(U_M - cr)$ in ms^{-1} for the case described in Fig. 19.

It shoud be stressed that the diagrams in Fig. 19 and Fig. 20 apply to the wind-profile in Fig. 13 as indicated by the dots and not to the linear wind-profile. The values of the growth rate and the phase speed will vary with the number of components included in the series expansion of $U(p_*)$. This can be seen from Fig. 21 and Fig. 22, in which the growth rate and the phase speed are plotted as a function of the number of components. It is seen that both quantities are increasing functions of n_s although the slope becomes steadily smaller as n_s increases. The curves apply to a single point in the diagram with $L = 1000$ km and $U_s = 40$ ms^{-1}. One conclusion is that the structure functions employed in this study are not very efficient in approximating a straight line.

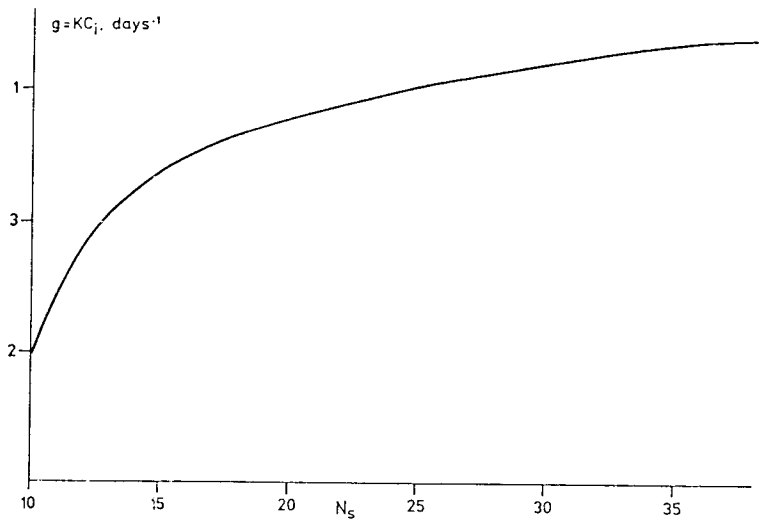

Fig. 21. The growth rate ($days^{-1}$) as a function of the number (n_s) of vertical components.

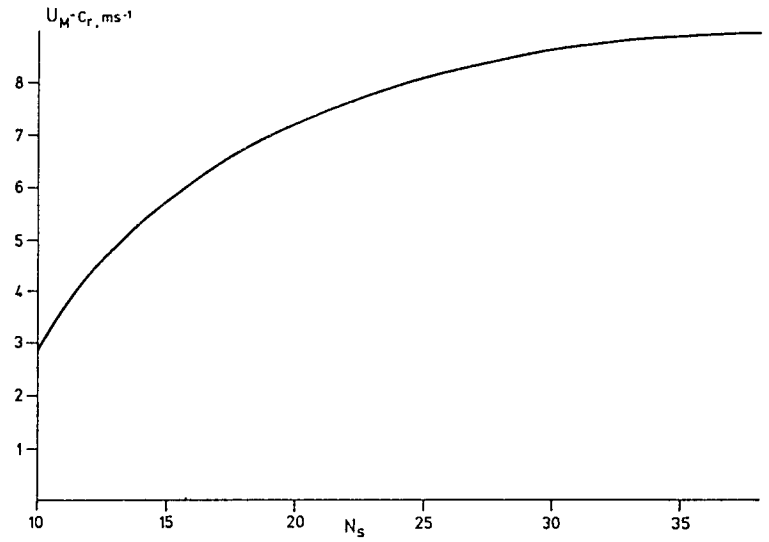

Fig. 22. $(U_M - cr)$, ms^{-1}, as a function of the number (ns) of vertical components.

Concerning the windprofiles there is, however, a much more important question. It is related to the comparison between the model described in this and one of previous sections. These will be considered in the following section.

5. Comparison with the continuous case

Charney and Stern (1962) made a detailed analysis of the stability of internal baroclinic atmospheric jet streams . The model which they used is somewhat more general than the cases treated in this paper because the zonal current is a function of both latitude and height. We can, however, easily reproduce the essential argument for our model, which is governed by the conservation of quasi -geostrophic, potential vorticity. Considering the zonal current $U = U(p_*)$ and perturbations of the form

$$\psi' = \hat{\psi} \exp\ (ik(x - ct)) \tag{5.1}$$

we find the frequency equation

$$\frac{d}{dp_*}\left[\frac{fo^2}{\bar{\sigma}p_o^2}\ \frac{d\hat{\psi}}{dp_*}\right] - k^2\hat{\psi} + \frac{\beta - \frac{d}{dp_*}(\frac{f_o^2}{\bar{\sigma}p_o^2}\frac{dU}{dP_*})}{U - c}\hat{\psi} = 0 \tag{5.2}$$

which in this investigation is to be solved under boundary conditions

$$\frac{d\hat{\psi}}{dp_*} = 0 \text{ for } p_* = p_T \text{ and } p_* = 1 \tag{5.3}$$

Writing $c = c_r + ic_i$, multiplying (5.2) by the complex conjugate of $\tilde{\psi}$ and integrating from p_T to 1 we find using (5.3) that

$$-\int_{p_T}^{1}\left[\frac{f_o^2}{\bar{\sigma}p_o^2}\mid\frac{d\hat{\psi}}{dp_*}\mid^2+k^2\mid\hat{\psi}\mid^2\right]dp_*+\int_{p_T}^{1}\frac{\beta-\frac{d}{dp_*}\left(\frac{f_o^2}{\bar{\sigma}p_o^2}\frac{dU}{dp_*}\right)}{(U-c_r)^2+c_i^2}\mid\hat{\psi}\mid^2 dp_*=0 \tag{5.4}$$

$$ic_i\int_{p_T}^{1}\frac{\beta-\frac{d}{dp_*}\left(\frac{f_o^2}{\bar{\sigma}p_*^2}\frac{dU}{dp_*}\right)}{(U-c_r)^2+c_i^2}\mid\hat{\psi}\mid^2 dp_*=0 \tag{5.5}$$

where

$$\mid\hat{\psi}\mid^2=\hat{\psi}\cdot\tilde{\psi} \tag{5.6}$$

From (5.5) it is seen that, if $c_i > 0$ it is required that the quantity

$$H(p_*)=\beta-\frac{d}{dp_*}\left[\frac{f_o^2}{\bar{\sigma}p_o^2}\frac{dU}{dp_*}\right] \tag{5.7}$$

must change sign somewhere in the interval from p_T to 1. If this is not the case, we can conclude from (5.5) that $c_i = 0$. We can thus say that a sufficient condition for stability is that $H(p_*)$ is of one sign in the interval from p_T to 1. On the other hand, if $H(p_*)$ does change sign we have the fulfillment of a necessary condition for instability.

Let us start with a linear wind-profile, say

$$U(p^*)=U_M+\frac{U_T}{1-p_T}\left[\frac{1}{2}(1+p_T)-p_*\right] \tag{5.8}$$

and with

$$\bar{\sigma}=\sigma_o p_*^{-2} \tag{5.9}$$

We find that

$$H(p_*)=\beta+\frac{f_o^2}{\sigma_o p_o^2}\frac{U_T}{1-p_T}\cdot 2p_* > 0 \tag{5.10}$$

which shows that the linear wind-profile is stable, when we consider the continuous case. However, in this paper we have all the time been dealing with a representation

$$U(p_*)=\sum_{q=1}^{Q}U(q)G_q(p_*) \tag{5.11}$$

in which case

$$H(p_*) = \beta + \sum_{q=1}^{Q} \lambda(q)^2 U(q) G_q(p_*) \tag{5.12}$$

For a given truncation, i.e. for a specific finite value of Q, it is no longer obvious that $H(p_*)$ does not change sign in the interval from p_T to 1. $H(p_*)$ can as a matter of fact change sing as one can see by calculating

$$H(1) = \beta - \sum_{q=1}^{Q} \lambda(q)^2 U(q) \cdot D(q) \cdot 2\mu(q) \tag{5.13}$$

and

$$H(p_T) = \beta - \sum_{q=1}^{Q} \lambda(q)^2 U(q) \frac{D(q)}{\sqrt{p_T}} 2\mu(q) \cos(q\Pi) \tag{5.14}$$

If $H(1)$ and $H(p_T)$ are of opposite sign, there is at least one zero of $H(p^*)$ between them. (5.13) and (5.14) have been calculated for various values of Q using the fact that for $U(q)$ we have

$$U(q) = U_T u(q) \tag{5.15}$$

where $u(q)$ are the coefficients for $U_T = 1$ ms^{-1}. For each truncation Q we have used values of U_T satisfying

$$1 \leq U_T \leq 100 \tag{5.16}$$

It turns out that for $Q > 10$ we find for all values of $U_T > 1$ (but not $U_T = 1$) that $H(1) < 0$ and $H(p_T) > 0$. The result is thus that for a given truncation and $U_T > 1$ the necessary condition for instability is satisfied. The actual, steady state solutions found by numerical integrations of the system (4.6) shows empirically (in view of (4.21) and (4.26)) that instability is also in fact present. The qualities $H(1) < 0$ and $H(p_T) > 0$ for sufficiently large U_T can be made plausible by writing (5.13) and (5.14) in the form

$$H(1) = \beta - U_T S_e - U_T S_o$$

$$H(p_T) = \beta - \frac{U_T}{\sqrt{p_T}} S_e + \frac{U_T}{\sqrt{p_T}} S_o \tag{5.17}$$

in which

$$S_e = \sum_{q=\text{even}} 2\lambda(q)^2 u(q) D(q) \mu(q)$$

$$S_o = \sum_{q=\text{odd}} 2\lambda(q)^2 u(q) D(q) \mu(q) \tag{5.18}$$

For a linearly increasing basic current all $u(q) > 0$, and it is thus seen $S_e > 0$ and $S_o > 0$. It is therefore obvious that $H(1) < 0$ for sufficiently large values of U_T. Since $S_e \simeq S_o$ for a given truncation, it is plausible that $H(p_T) > 0$. The example shows the difference which may exist between a continuous case and a case with restricted vertical resolution.

The linear wind-profile is of course a very special case. It may therefore be of some importance to consider more general cases. For this purpose we may reconsider the wind-profiles from section 2, i.e. eq. (2.24). For this definition we may calculate $H(p_*)$ which becomes

$$H(p_*) = \beta_* - \frac{f_o^2}{\sigma_o p_o^2} \frac{U_m}{N(\alpha,\ \beta)} \frac{p_*(p_* - p_T)^{\alpha-2}(1 - p_*)^{\beta-2}}{(1 - p_T)^{\alpha+\beta}} h(p_*) \tag{5.19}$$

where

$$h(p_*) = (\alpha + \beta)(\alpha + \beta + 1)p_*^3 - 2(\alpha + \beta p_T + 1 + p_T)p_*^2$$

$$+[(\alpha + \beta p_T)(\alpha + \beta p_T + 1 + p_T) + 3p_T(\alpha + \beta)]p_* - 2p_T(\alpha + \beta p_T) \tag{5.20}$$

We notice that when $\alpha \geq 2$ and $\beta \geq 2$ then $H(p_*) = \beta_*$ for $p_* = p_T$ and $p_* = 1$. Fig. 23 shows $H(p_*)$ for $U_m = 4$ which is the smallest value for which the function changes sign twice.

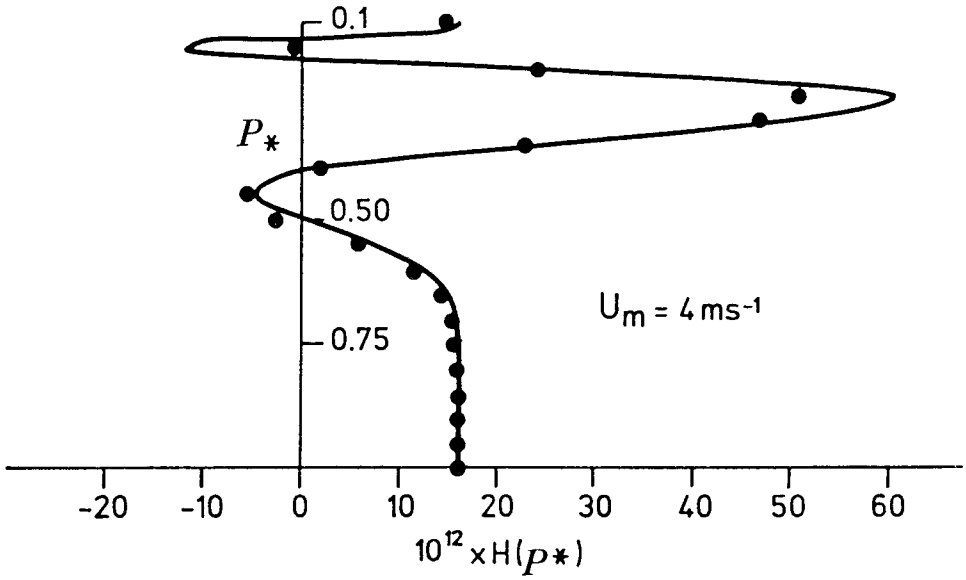

Fig. 23. The curve is the meridional derivative of the absolute, quasi-geostrophic, potential vorticity. The dots are obtained by adding the contributions from 30 vertical components.

The function has the same general shape for larger values of U_m. We may thus conclude that the jet-shaped wind-profile satisfies the necessary condition for instability. On Fig. 23 we have also included values of $H(p_*)$ as calculated by the spectral representation, i.e.

$$H(p_*) = \beta + \sum_{q=1}^{30} \lambda(q)^2 \cdot U(q) \cdot G_q(p_*) \tag{5.21}$$

These values indicated by dots on the figure show that the representation (5.21) is quite good although as expected it does not represent sharp maxima and minimum exactly.

6. Concluding remarks

The main topic of this and the previous two papers has been the determination of the structure of transient baroclinic waves. In the present paper we have concentrated on a continuous vertical distribution as determined by a set of vertical structure functions. For these functions, and thus for the parameters developed in a series representation of them, we have adopted the simplified lower boundary condition of $\omega = 0$ corresponding to a vanishing value of the vertical derivative at the boundary. It is not necessary to do this, and we could just as well have used the boundary condition of a vanishing vertical velocity as done for examply by Kasahara and Tanaka (1989). However, some simplifications in the equations are obtained by the adopted boundary condition, and any significant change is in the basic mode only.

Steady state solutions are obtained to equations describing the time development of the relative amplitude and the relative phase angle by a time-integration scheme. We stress once again that this does not mean a description of stationary waves, but a determination of the asymptotic structure, because in the steady state the ratio of the wave amplitude at an arbitrary pressure level and the same quantity for the vertical average does not change. The same can be said for the difference in phase angle at an arbitrary level and the same quantity for the vertical mean.

The process described above will converge only for baroclinic, growing waves. However, once a steady state solution is obtained, it can be used to determine both the real and the imaginary part of the phase speed. The procedure is therefore another way of solving a baroclinic stability problem for an arbitrary windprofile $U = U(p)$. In this regard, the procedure has the distinct advantage that the phase speed is determined in a unique fashion, and we are therefore finding the structure and the phase speed for the dominant component.

The vertical variations of the relative amplitude and phase vary greatly with the horizontal wavelength and with the related degree of instability, but the result is in general agreement with the conclusions from other related studies using different procedures. It turns out, however, that the real part of the phase speed and the growth rate are sensitive to the number of vertical structure functions used in the truncated system. On the other hand, the relative structure is rather insensitive to the truncation as long as a reasonable number of these functions are used.

The procedure used to describe vertical variations (the structure functions) require a finite number of functions. This feature leads to a comparison between the truly continuous case and the approximation to it by the use of a finite set of functions. It is shown that distinct differences may exist between the two cases.

REFERENCES

Abramowitz, M. and I. Stegun, 1964. Handbook of Mathematical Functions, *Appl. Math. Series*, No. 55, National Bureau of Standards, Washington D.C., 1046 p.

Brown, J. A. Jr., 1969. A numerical investigation of hydrodynamic instability and energy convections in the quasi -geostrophic atmosphere, Part 1 and II, *Jour. of Atmos. Sc.*, **26**, 352-375.

Charney, J. G. and N. E. Stern, 1962. On the stability of internal baroclinic jets in a rotating atmosphere, *Jour. of Atmos. Sc.*, **19**, 159-172.

Gates, W. L., 1961. Static stability measures in the atmosphere, *Jour. of Meteor.*, **18**, 526-533.

Green, J. S. A, 1960. A problem in baroclinic stability, *Quart. Jour. Roy. Met . Soc.* **86**, 237-251.

Jacobs, S. J. and A. Wiin-Nielsen, 1966. On the stability of a barotropic, basic flow in a stratified atmosphere, *Jour. Atmos. Sci.*, **23**, 682-687.

Kasahara, A. and H. L. Tanaka, 1989. Application of vertical normal mode expansion to problems of baroclinic instability, *Jour. Atmos. Sci.*, **6**, 489-510.

Lorenz, E. N. , 1967. The nature and theory of the general circulation of the atmosphere, *World Meteor. Organization*,

Wiin-Nielsen, A., 1962. On transformation of kinetic energy between the vertical shear flow and the vertical mean flow in the atmosphere, *Mon. Wea. Rev.* **90,** 311-323.

Wiin-Nielsen, A. , 1971. On the motion of various vertical modes of transient very long waves, *Tellus,* **23**, 87-98.

Wiin-Nielsen, A., 1989. On the structure of transient, atmospheric waves, Part I, *Atmósfera*, **2**, 3-15.

Wiin-Nielsen, A., 1989. On the structure of transient, atmospheric waves, Part II, *Atmósfera*, **2**, 189-208.